Four-dimensional anisotropic mesh adaptation for spacetime numerical simulations

Philip Claude Caplan

Thesis committee: Prof. David L. Darmofal (chair), Bob Haimes, Prof. Jaime Peraire

PhD Thesis Defense

17 May 2019

Introduction

MIT AEROASTRO

We want accurate answers to PDEs using numerical simulations.

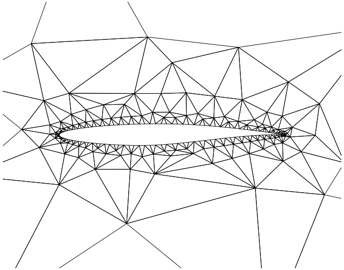

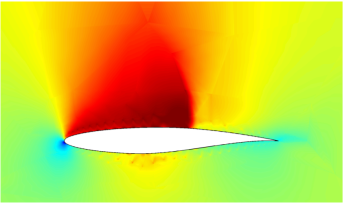

783% error in drag

We want accurate answers to PDEs using numerical simulations.

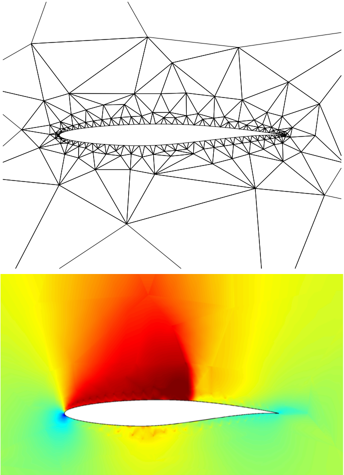

783% error in drag

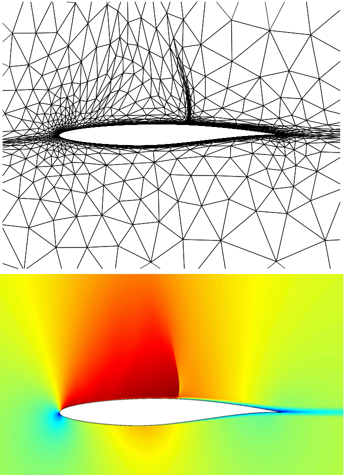

0.5% error in drag

"The number of wings designed and wind tunnel tested has steadily decreased." **[Johnson, 2005]**

"The number of wings designed and wind tunnel tested has steadily decreased." [Johnson, 2005]

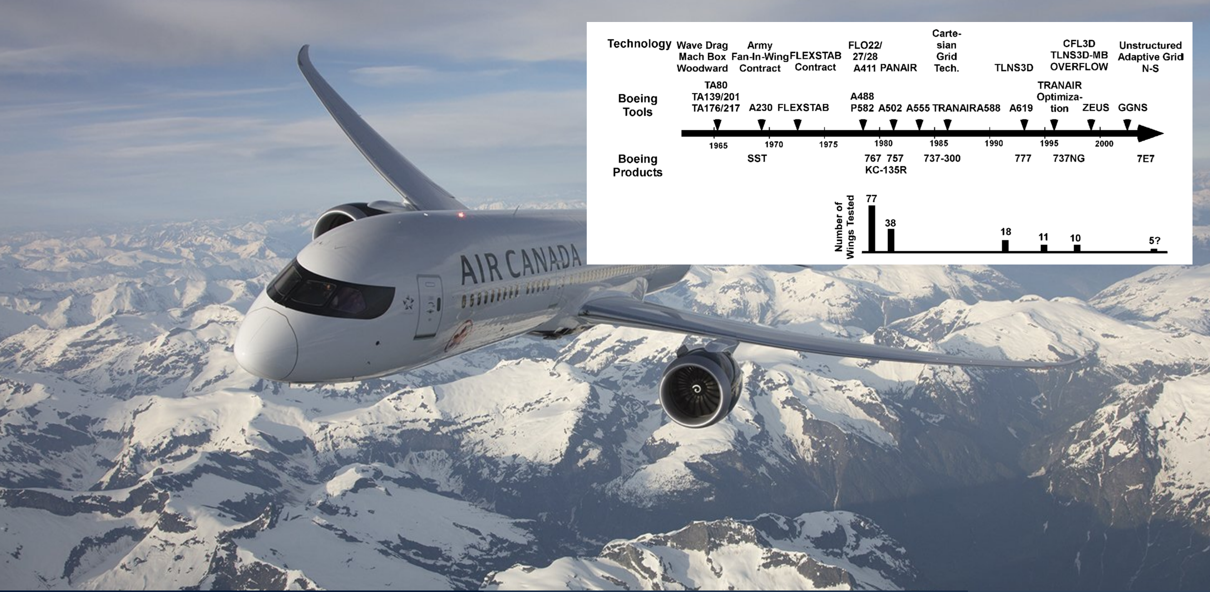

Mesh adaptation is useful for obtaining accurate solutions.

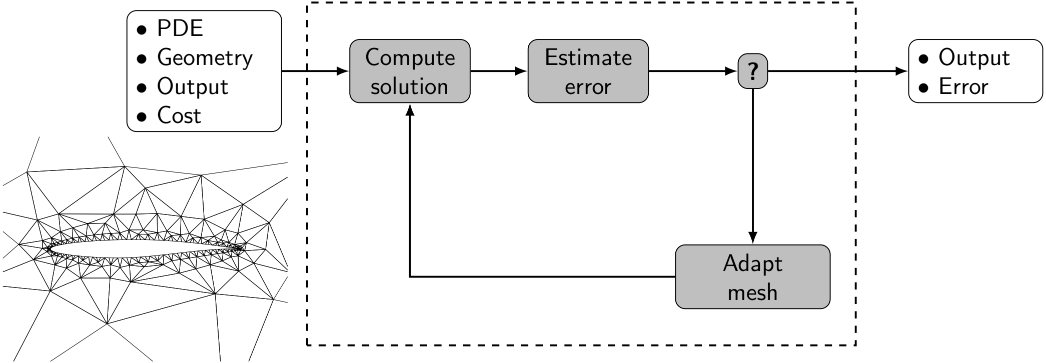

Mesh adaptation is useful for obtaining accurate solutions.

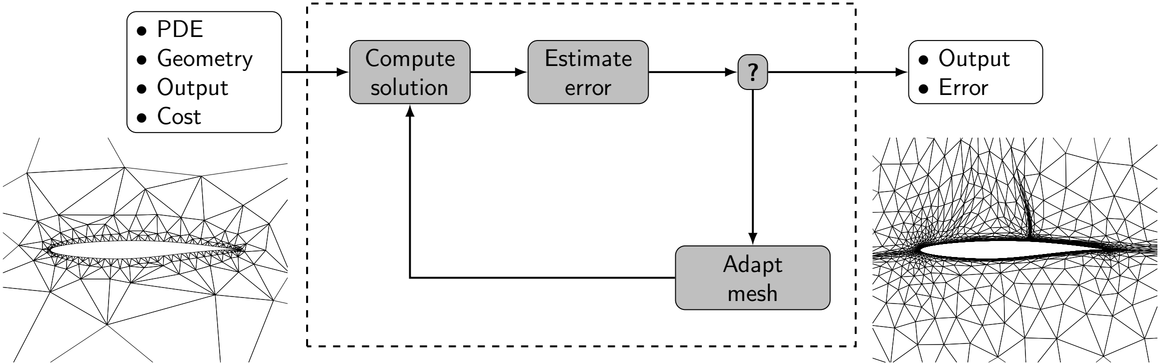

How to solve problems with time-dependent features?

[Song, 2014]

Time-marching approach is computationally expensive.

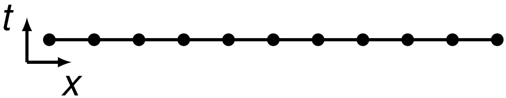

Time-marching approach is computationally expensive.

MIT AEROASTRO

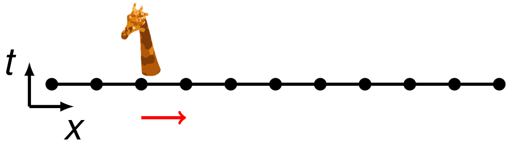

Time-marching approach is computationally expensive.

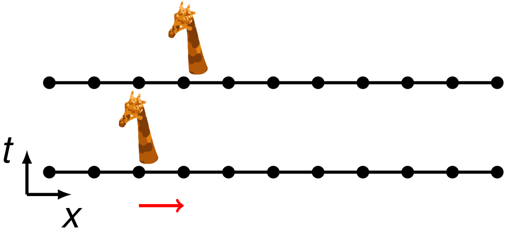

Time-marching approach is computationally expensive.

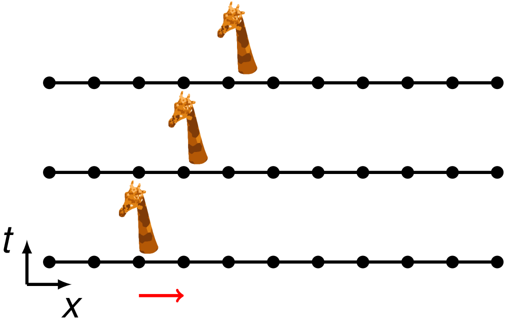

Time-marching approach is computationally expensive.

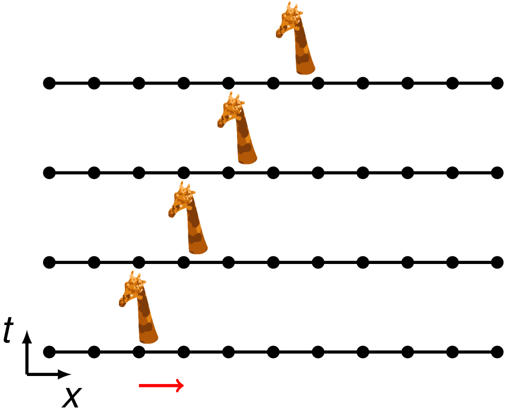

Time-marching approach is computationally expensive.

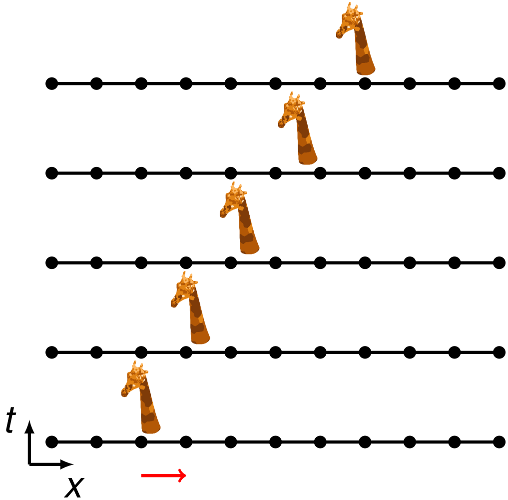

Time-marching approach is computationally expensive.

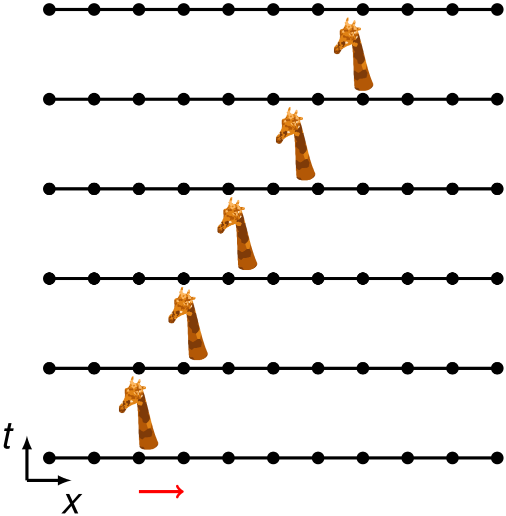

Time-marching approach is computationally expensive.

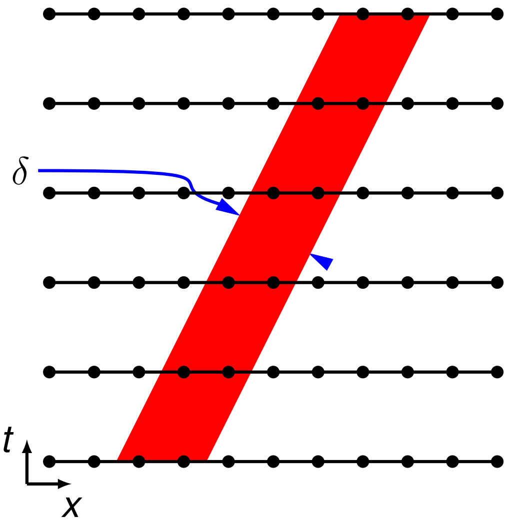

Spacetime uniform refinement requires $\mathcal{O}(\delta^{-2})$ elements.

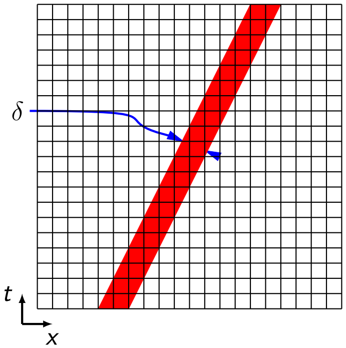

Uniform $\mathcal{O}(\delta^{-2})$

Spacetime tensor-product approach requires $\mathcal{O}(\delta^{-1})$ elements.

[Bangerth, 1999]
[Hartmann, 2001]

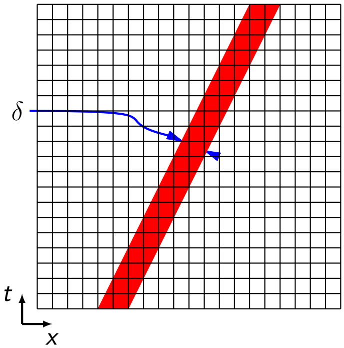

Uniform $\mathcal{O}(\delta^{-2})$

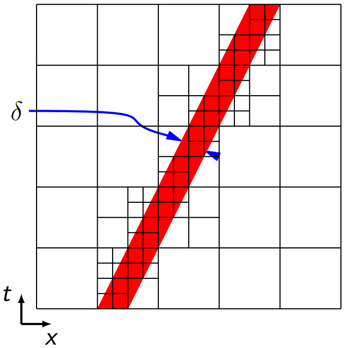

Tensor-product $\mathcal{O}(\delta^{-1})$

Spacetime unstructured approach requires $\mathcal{O}(1)$ elements.

[Bangerth, 1999]
[Hartmann, 2001]

[Yano, 2012]

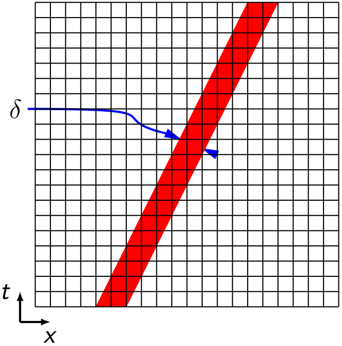

Uniform $\mathcal{O}(\delta^{-2})$

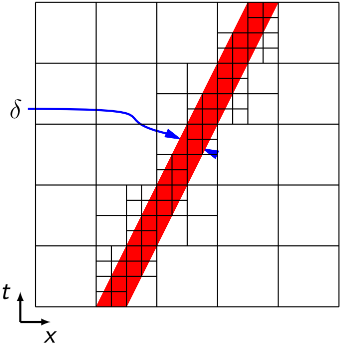

Tensor-product $\mathcal{O}(\delta^{-1})$

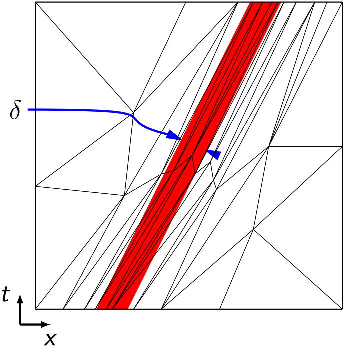

Unstructured $\mathcal{O}(1)$

Spacetime unstructured approach demonstrated in $1d + t$ and $2d + t$.

[Yano, 2012]

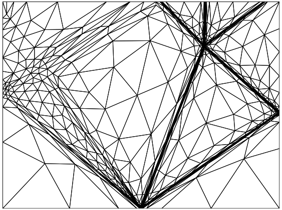

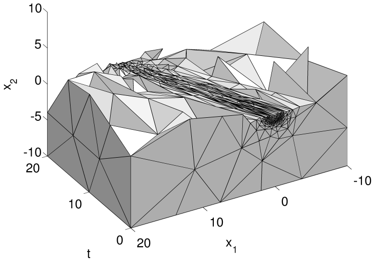

[Jayasinghe, 2018]

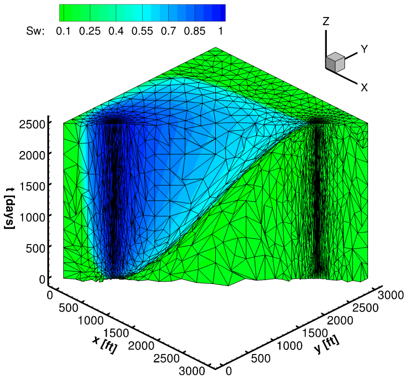

Spacetime unstructured approach demonstrated in $1d + t$ and $2d + t$.

[Yano, 2012]

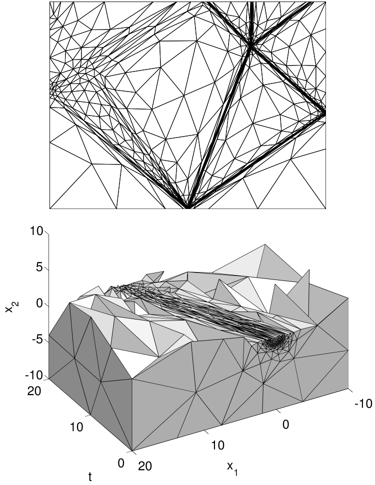

[Jayasinghe, 2018]

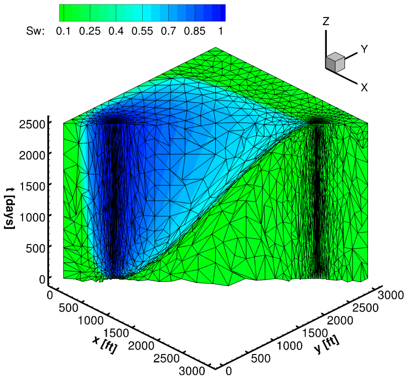

We need unstructured anisotropic $4d$ meshes for unsteady $3d$ problems.

Anisotropic meshes can be obtained using a metric field.

MIT AEROASTRO

Optimize mesh?

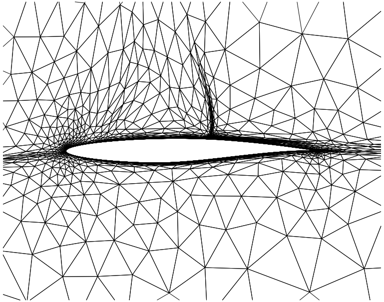

$\mathcal{M}$: mesh

$$\mathcal{M}^* = \arg\min_{\mathcal{M}} \underbrace{E(\mathcal{M})}_{\text{error}} \quad \text{such that} \quad \underbrace{C(\mathcal{M})}_{\text{cost}} \leq c_t$$

Anisotropic meshes can be obtained using a metric field.

Optimize mesh?

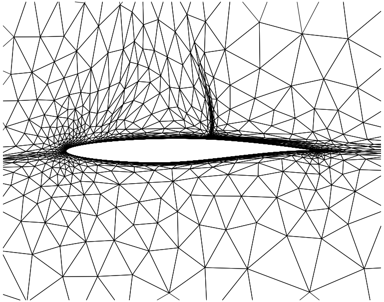

$\mathcal{M}$: mesh

$$\mathcal{M}^* = \arg\min_{\mathcal{M}} \underbrace{E(\mathcal{M})}_{\text{error}} \quad \text{such that} \quad \underbrace{C(\mathcal{M})}_{\text{cost}} \leq c_t$$

Optimize metric field? [Loseille, 2011]

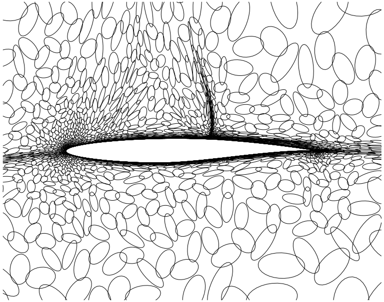

$\mathbf{m}$: metric field

$$\mathbf{m}^* = \arg\min_{\mathbf{m}} \underbrace{E(\mathbf{m})}_{\text{error}} \quad \text{such that} \quad \underbrace{C(\mathbf{m})}_{\text{cost}} \leq c_t$$

Anisotropic meshes can be obtained from a metric-conforming mesher.

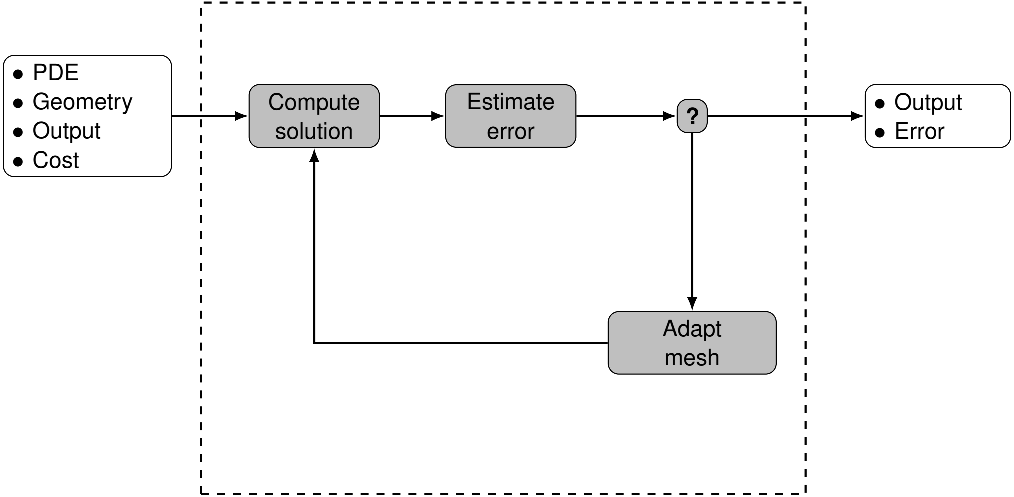

Anisotropic meshes can be obtained from a metric-conforming mesher.

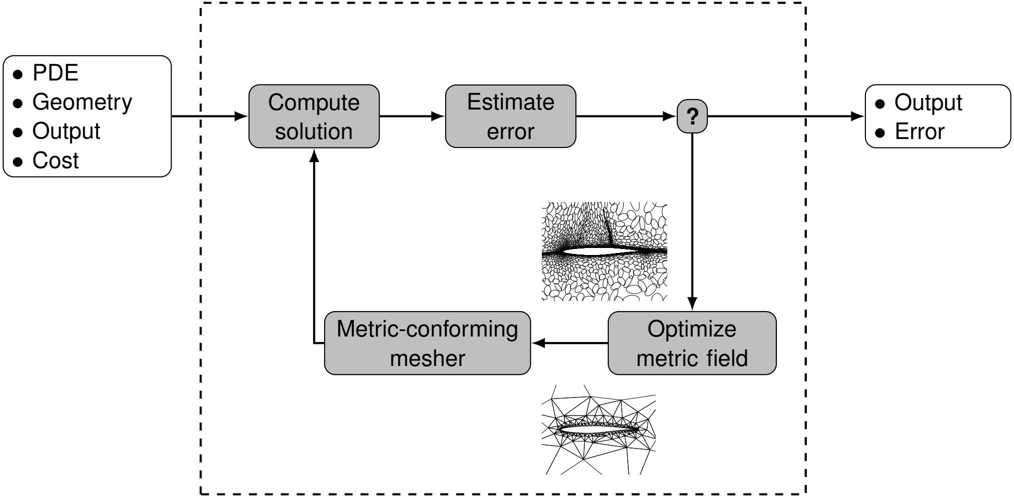

Anisotropic meshes can be obtained from a metric-conforming mesher.

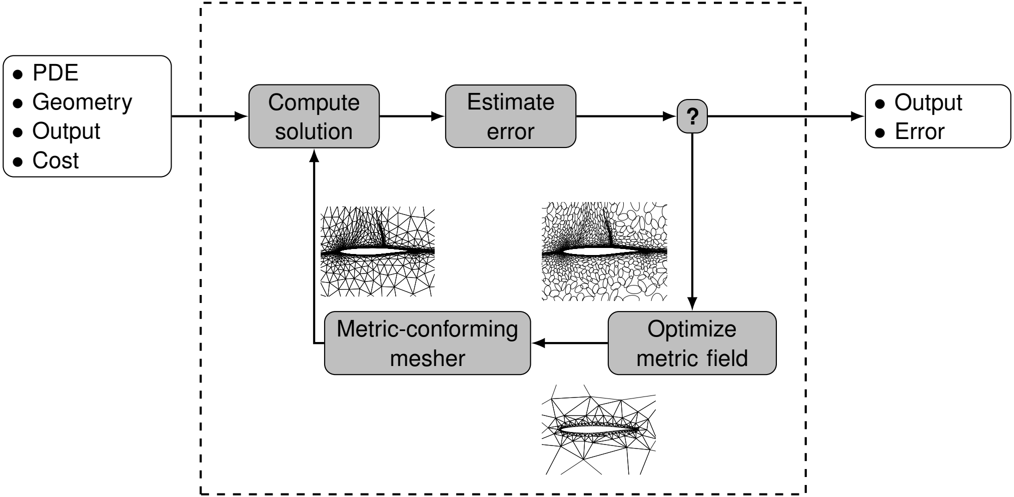

Previous attempts at anisotropic $4d$ meshing were not successful.

[Coupez, 2000] & **[Gruau, 2005]**

- Star operator for local mesh operations,
- Minimum volume principle,
- Uniform metric fields.

h	time (s)	# vertices	# elements
1/2	4	126	946
1/3	41	451	4573
1/4	179	1192	14887
1/5	547	2588	35894

[Tremblay, 2007]

- *Simulated* edge swapping,
- Poor metric-conformity (aspect ratio 10:1),
- Heat equation in $3d+t$ with isotropic meshes.

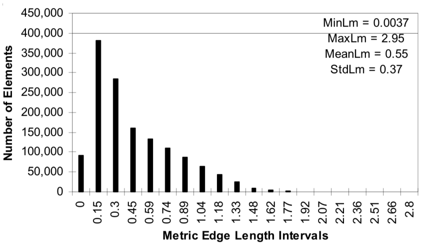

Previous attempts at anisotropic $4d$ meshing were not successful.

[Coupez, 2000] & **[Gruau, 2005]**

- Star operator for local mesh operations,
- Minimum volume principle,
- Uniform metric fields.

h	time (s)	# vertices	# elements
1/2	4	126	946
1/3	41	451	4573
1/4	179	1192	14887
1/5	547	2588	35894

[Tremblay, 2007]

- *Simulated* edge swapping,
- Poor metric-conformity (aspect ratio 10:1),
- Heat equation in $3d+t$ with isotropic meshes.

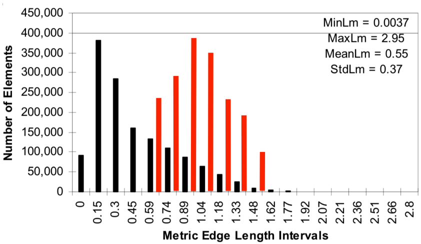

Previous attempts at anisotropic $4d$ meshing were not successful.

[Coupez, 2000] & **[Gruau, 2005]**

- Star operator for local mesh operations,
- Minimum volume principle,
- Uniform metric fields.

h	time (s)	# vertices	# elements
1/2	4	126	946
1/3	41	451	4573
1/4	179	1192	14887
1/5	547	2588	35894

[Tremblay, 2007]

- *Simulated* edge swapping,
- Poor metric-conformity (aspect ratio 10:1),
- Heat equation in $3d+t$ with isotropic meshes.

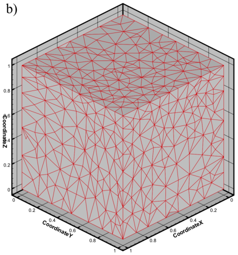

Thesis objectives & contributions

Main objective:

Develop an anisotropic four-dimensional meshing capability for adaptive numerical simulations.

Approach:

- Simplex meshes (triangles, tetrahedra, pentatopes).
- Local cavity operator framework.
- Mesh Optimization via Error Sampling and Synthesis.

Contributions:

(1) Develop an algorithm and software for 4d **metric-conforming mesh adaptation**.

(2) **Validate the adaptive algorithm** on 4d problems.

(3) Demonstrate first **PDE-driven anisotropic** unstructured adaptation for **unsteady** 3d **problems**.

Four-dimensional anisotropic mesh adaptation algorithm

MIT AEROASTRO

Metric-conforming mesher strives to create unit n-simplices.

Goals for a mesh $\mathcal{M} = (\mathcal{V}, \mathcal{T})$ of $\Omega \subset \mathbb{R}^n$

- Edge lengths are 1:

$$\ell_{\mathbf{m}}(e) = 1, \ \forall e \in \mathcal{E}(\mathcal{T})$$

- Quality is that of equilateral simplex:

$$q_{\mathbf{m}}(\boldsymbol{\kappa}) = \frac{1}{q_{\Delta}} \frac{v_{\mathbf{m}}^{2/n}(\boldsymbol{\kappa})}{\sum_{e \in \mathcal{E}(\kappa)} \ell_{\mathbf{m}}^2(e)} = 1, \ \forall \kappa \in \mathcal{T}$$

- # simplices matches metric field complexity:

$$n_s v_{\Delta} = \int_{\mathcal{M}} \sqrt{\det \mathbf{m}} \, \mathrm{d}\mathbf{x}$$

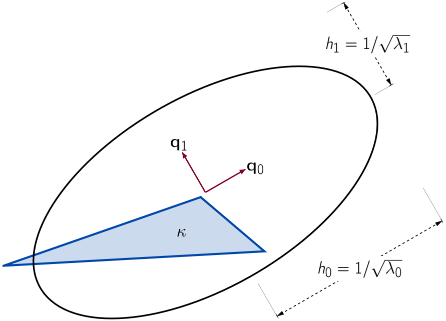

Metric-conforming mesher strives to create unit n-simplices.

Goals for a mesh $\mathcal{M} = (\mathcal{V}, \mathcal{T})$ of $\Omega \subset \mathbb{R}^n$

- Edge lengths are close to 1:

$$1/\sqrt{2} \leq \ell_{\mathbf{m}}(e) \leq \sqrt{2}, \ \forall e \in \mathcal{E}(\mathcal{T})$$

- Quality is close to that of equilateral simplex:

$$q_{\mathbf{m}}(\boldsymbol{\kappa}) = \frac{1}{q_\Delta} \frac{v_{\mathbf{m}}^{2/n}(\boldsymbol{\kappa})}{\sum_{e \in \mathcal{E}(\kappa)} \ell_{\mathbf{m}}^2(e)} \in [0.8, 1], \ \forall \kappa \in \mathcal{T}$$

- # simplices matches metric field complexity:

$$n_s v_\Delta \approx \int_{\mathcal{M}} \sqrt{\det \mathbf{m}}\, \mathrm{d}\mathbf{x}$$

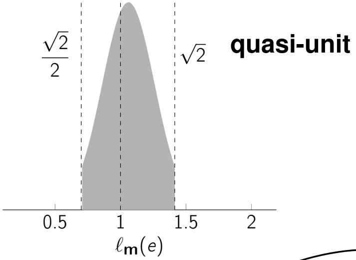

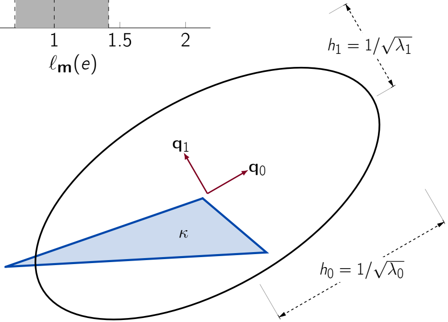

Local operators modify an existing mesh to meet target criteria.

Local operators modify an existing mesh to meet target criteria.

Split

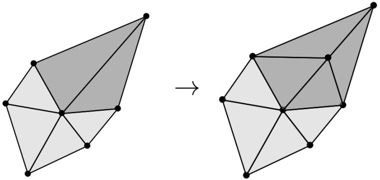

Local operators modify an existing mesh to meet target criteria.

Split

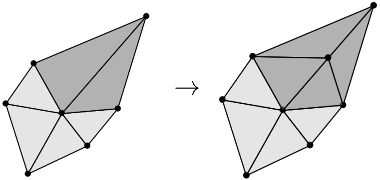

Collapse

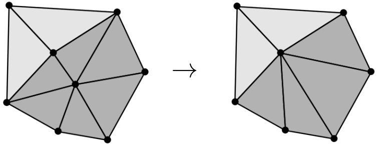

Local operators modify an existing mesh to meet target criteria.

Split

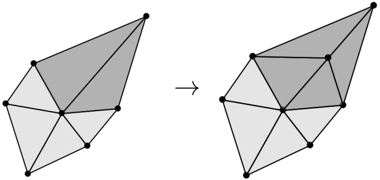

Smoothing

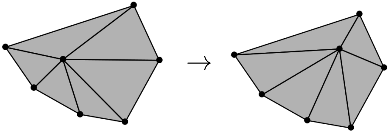

Collapse

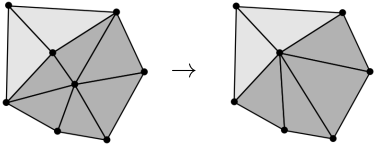

Local operators modify an existing mesh to meet target criteria.

Split

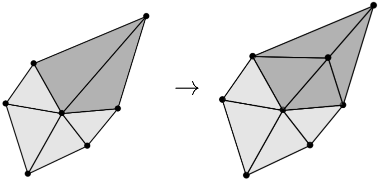

Smoothing

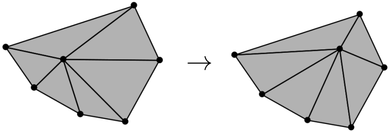

Collapse

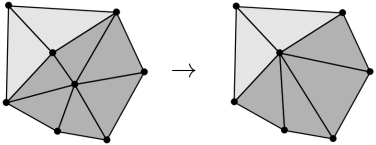

Swap

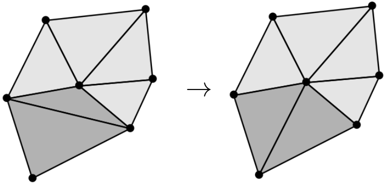

Local operators can be viewed in a dimension-independent way.

Application of mesh modification operator: **[Coupez, 2000]**,**[Loseille, 2017]**

$$\mathcal{T}^{k+1} = \mathcal{T}^k \setminus \underbrace{\mathcal{C}(f)}_{\text{cavity}} \cup \underbrace{\mathcal{B}(p, \partial\mathcal{C}^k)}_{\text{insertion}}$$

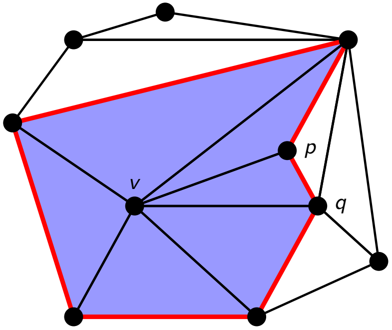

Local operators can be viewed in a dimension-independent way.

Application of mesh modification operator: **[Coupez, 2000]**,**[Loseille, 2017]**

$$\mathcal{T}^{k+1} = \mathcal{T}^{k} \setminus \underbrace{\mathcal{C}(f)}_{\text{cavity}} \cup \underbrace{\mathcal{B}(p, \partial\mathcal{C}^{k})}_{\text{insertion}}$$

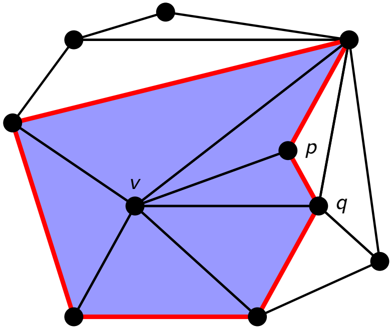

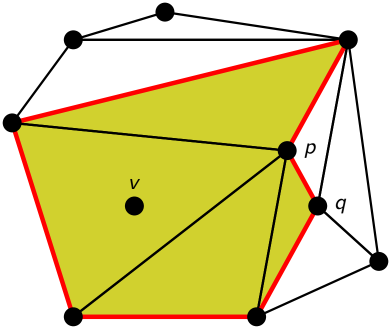

Local operators can be viewed in a dimension-independent way.

Application of mesh modification operator: **[Coupez, 2000]**,**[Loseille, 2017]**

$$\mathcal{T}^{k+1} = \mathcal{T}^k \setminus \underbrace{\mathcal{C}(f)}_{\text{cavity}} \cup \underbrace{\mathcal{B}(p, \partial\mathcal{C}^k)}_{\text{insertion}}$$

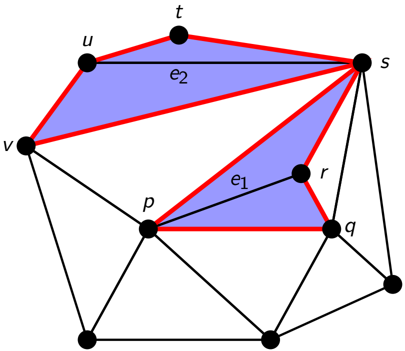

Local operators can be viewed in a dimension-independent way.

Application of mesh modification operator: **[Coupez, 2000]**,**[Loseille, 2017]**

$$\mathcal{T}^{k+1} = \mathcal{T}^{k} \setminus \underbrace{\mathcal{C}(f)}_{\text{cavity}} \cup \underbrace{\mathcal{B}(p, \partial\mathcal{C}^{k})}_{\text{insertion}}$$

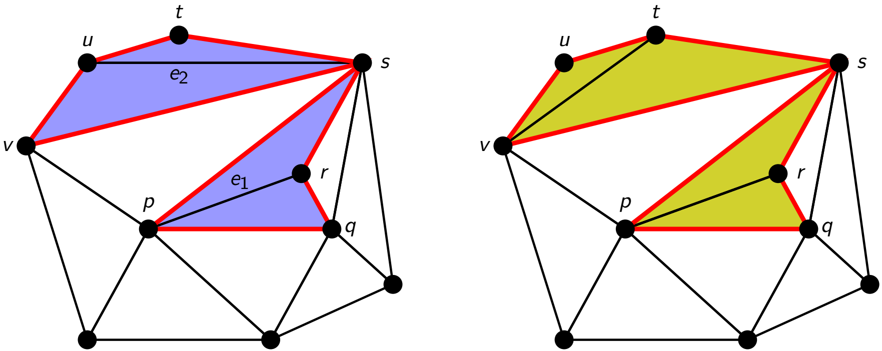

Operator schedule progressively tries to improve metric conformity.

adaptMesh

input: $\mathcal{M}_{\text{in}} = (\mathcal{V}_{\text{in}}, \mathcal{T}_{\text{in}})$, $\mathbf{m}$
output: $\mathcal{M}_{\text{out}}$ (modified)

$\triangleright$ **stage 1:** target edges longer than 2
$\mathcal{M} \leftarrow$ **collapseEdges**$(\mathcal{M}, \mathbf{m})$
$\mathcal{M} \leftarrow$ **splitEdges**$(\mathcal{M}, \mathbf{m}, 2)$
$\mathcal{M} \leftarrow$ **swapEdges**$(\mathcal{M}, \mathbf{m})$
$\mathcal{M} \leftarrow$ **smoothVertices**$(\mathcal{M}, \mathbf{m})$

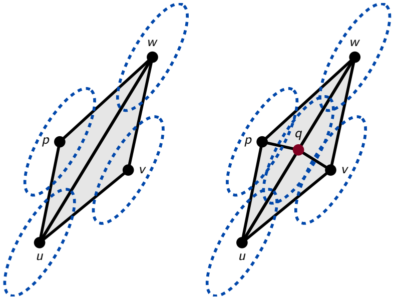

Operator schedule progressively tries to improve metric conformity.

adaptMesh

input: $\mathcal{M}_{\text{in}} = (\mathcal{V}_{\text{in}}, \mathcal{T}_{\text{in}})$, $\mathbf{m}$
output: $\mathcal{M}_{\text{out}}$ (modified)

$\triangleright$ **stage 2:** target edges longer than $\sqrt{2}$
$\mathcal{M} \leftarrow$ **collapseEdges**$(\mathcal{M}, \mathbf{m})$
$\mathcal{M} \leftarrow$ **splitEdges**$(\mathcal{M}, \mathbf{m}, \sqrt{2})$
$\mathcal{M} \leftarrow$ **swapEdges**$(\mathcal{M}, \mathbf{m})$
$\mathcal{M} \leftarrow$ **smoothVertices**$(\mathcal{M}, \mathbf{m})$

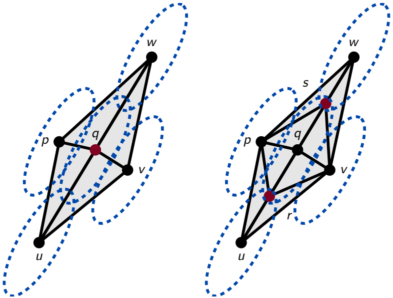

Operator schedule progressively tries to improve metric conformity.

MIT AEROASTRO

adaptMesh

input: $\mathcal{M}_{\text{in}} = (\mathcal{V}_{\text{in}}, \mathcal{T}_{\text{in}})$, $\mathbf{m}$
output: $\mathcal{M}_{\text{out}}$ (modified)

$\triangleright$ **stage 2:** target edges longer than $\sqrt{2}$
$\mathcal{M} \leftarrow$ **collapseEdges**$(\mathcal{M}, \mathbf{m})$
$\mathcal{M} \leftarrow$ **splitEdges**$(\mathcal{M}, \mathbf{m}, \sqrt{2})$
$\mathcal{M} \leftarrow$ **swapEdges**$(\mathcal{M}, \mathbf{m})$
$\mathcal{M} \leftarrow$ **smoothVertices**$(\mathcal{M}, \mathbf{m})$

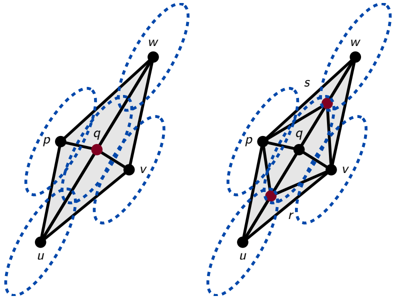

Highlights:

- do not create short edges during splits
- check number of pentatopes matches metric volume in $4d$

Demonstration with analytic metrics

MIT AEROASTRO

The meshing algorithm performs well on $3d$ benchmark cases.

Benchmarks of the Unstructured Grid Adaptation Working Group (UGAWG) **[Ibanez et al., 2017]**:

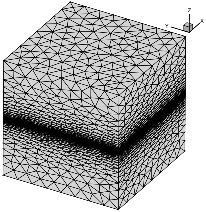

Cube Linear

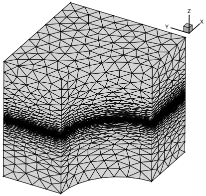

Cube-Cylinder Linear

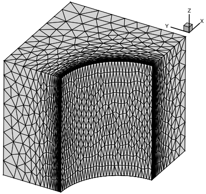

Cube-Cylinder Polar 2

The meshing algorithm performs well on 3d benchmark cases.

Benchmarks of the Unstructured Grid Adaptation Working Group (UGAWG) **[Ibanez et al., 2017]**:

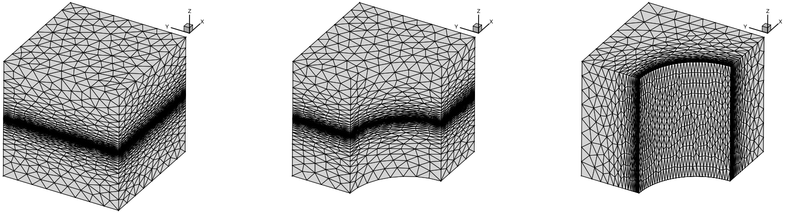

Cube Linear | Cube-Cylinder Linear | Cube-Cylinder Polar 2

`feflo.a` `EPIC-ICSM` `Omega_h`

The meshing algorithm performs well on 3*d* benchmark cases.

Benchmarks of the Unstructured Grid Adaptation Working Group (UGAWG) **[Ibanez et al., 2017]**:

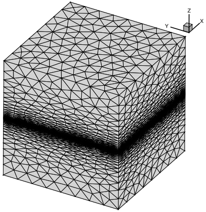

Cube Linear

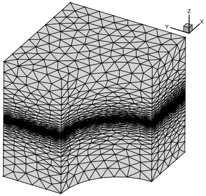

Cube-Cylinder Linear

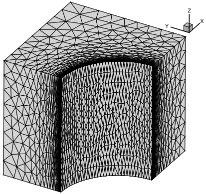

Cube-Cylinder Polar 2

`feflo.a` `EPIC-ICSM` `Omega_h` `avro`


RL 201

Assessment of metric-conformity.

% quasi-unit edge lengths

$$1/\sqrt{2} \leq \ell_{\mathbf{m}}(e) \leq \sqrt{2}$$

% quasi-unit simplices

$$q_{\mathbf{m}}(\kappa) > 0.8$$

 # simplices

$$n_s v_\Delta \approx \int \sqrt{\det \mathbf{m}}\, \mathrm{d}\mathbf{x}$$

Length and quality histograms will be plotted on logarithmic scales.

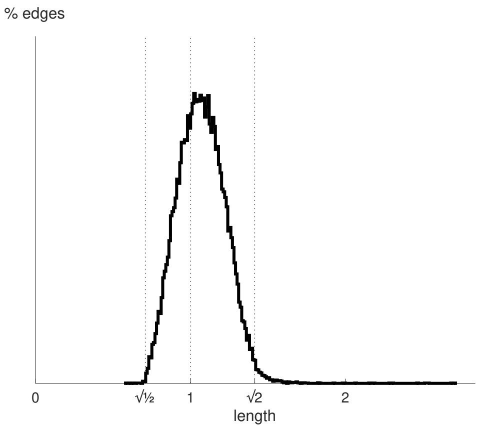

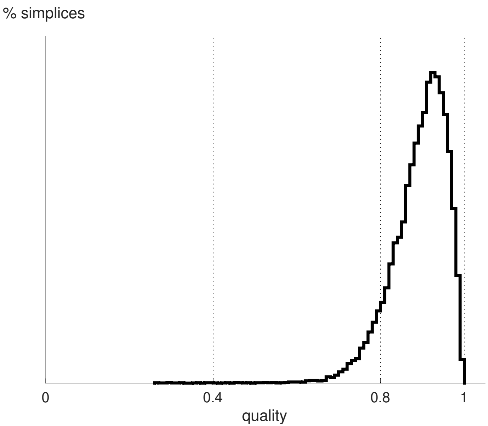

Length and quality histograms will be plotted on logarithmic scales.

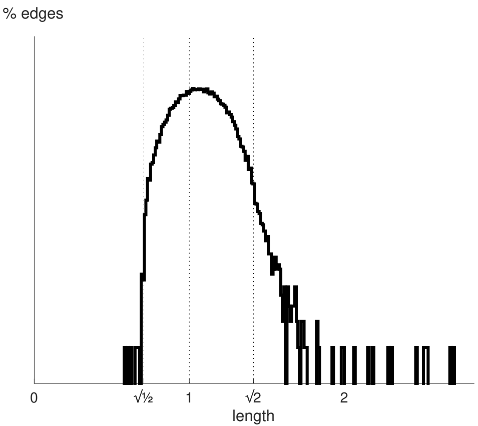

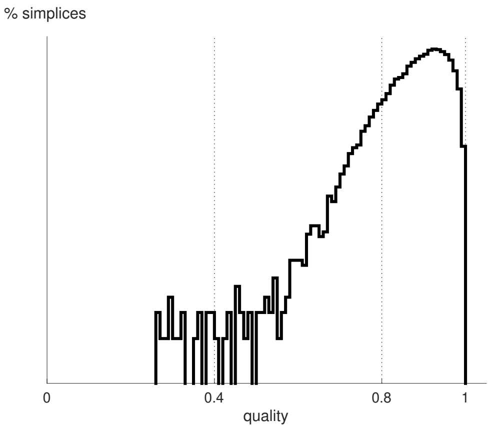

Expect 39k tetrahedra for the Cube Linear case.

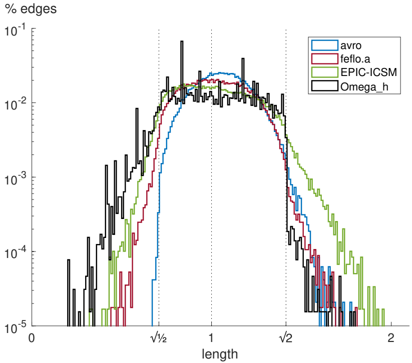

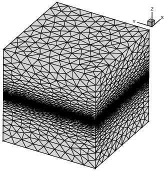

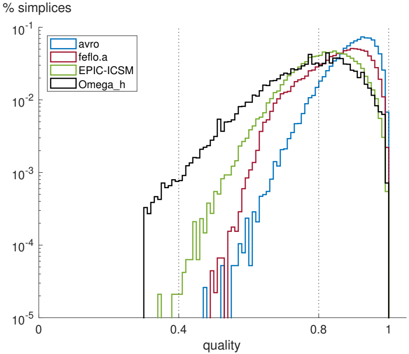

	$\%\ell_{\text{unit}}$	$\%q_{\text{unit}}$	# simplices
avro	99.10 %	92.15 %	38.30k
feflo.a	98.28 %	74.28 %	45.16k
EPIC-ICSM	93.04 %	59.52 %	47.55k
Omega_h	93.00 %	47.15 %	51.67k

Expect 31.7k tetrahedra for the Cube-Cylinder Linear case.

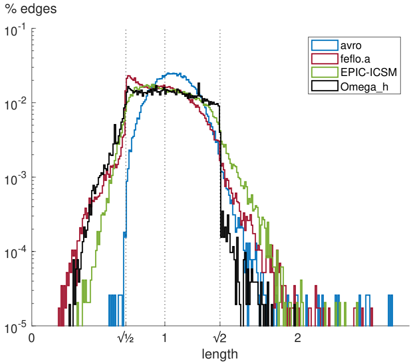

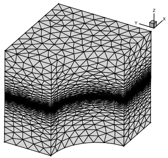

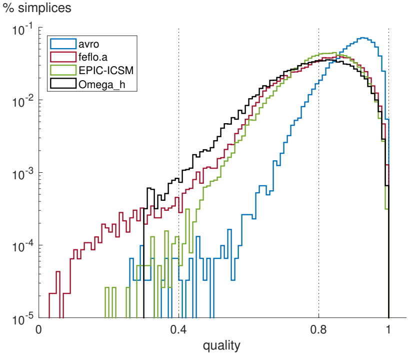

	$\%\ell_{\text{unit}}$	$\%q_{\text{unit}}$	# simplices
avro	98.79 %	90.88 %	30.45k
feflo.a	93.73 %	55.65 %	46.29k
EPIC-ICSM	92.07 %	56.71 %	38.30k
Omega_h	92.79 %	47.30 %	40.96k

Expect 36.4k tetrahedra for the Cube-Cylinder Polar 2 case.

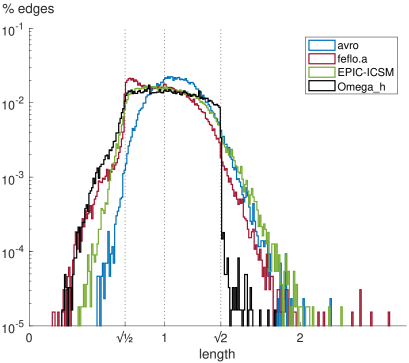

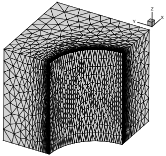

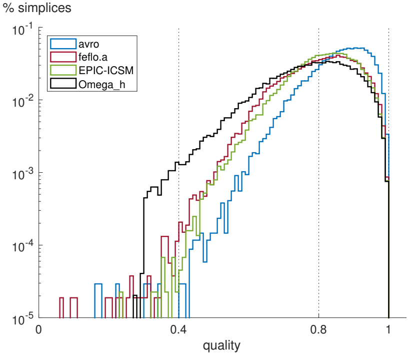

	$\%\ell_{\text{unit}}$	$\%q_{\text{unit}}$	# simplices
avro	95.76 %	78.76 %	34.20k
feflo.a	93.83 %	55.92 %	53.12k
EPIC-ICSM	91.77 %	58.52 %	44.28k
Omega_h	92.19 %	44.96 %	49.15k

Let's look at some $4d$ metric-conforming cases in a tesseract.

Tesseract Linear

$$\mathbf{m}(\mathbf{x}) = \mathrm{diag}\left(h_x^{-2}, h_y^{-2}, h_z^{-2}, h_t^{-2}\right)$$

$h_x = h_y = h_z = h =$ constant
h_t increases away from $t = 0.5$.

TL1 ($h = 0.25$) **TL2** ($h = 0.125$)

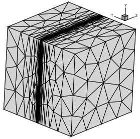

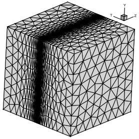

Tesseract Wave

$$\mathbf{m}(\mathbf{x}) = \mathbf{Q}\,\mathrm{diag}\left(h_r^{-2}, h_\theta^{-2}, h_\phi^{-2}, h_t^{-2}\right)\mathbf{Q}^t$$

Wave radius increases at $R(t) = R_0 + v_w t$
h_r increases away from $R(t)$, $h_t =$ constant
h_ϕ, h_θ similar to Cube-Cylinder Polar 2 case

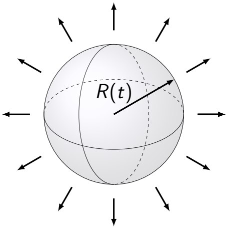

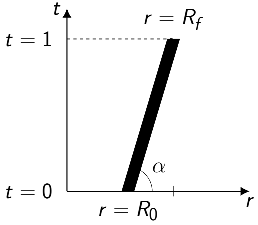

Let's look at some 4d metric-conforming cases in a tesseract.

Tesseract Linear

$$\mathbf{m}(\mathbf{x}) = \mathrm{diag}\left(h_x^{-2}, h_y^{-2}, h_z^{-2}, h_t^{-2}\right)$$

$h_x = h_y = h_z = h =$ constant
h_t increases away from $t = 0.5$.

TL1 ($h = 0.25$) **TL2** ($h = 0.125$)

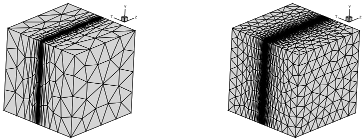

Refine hyperplanes at non-constant t.

Tesseract Wave

$$\mathbf{m}(\mathbf{x}) = \mathbf{Q}\,\mathrm{diag}\left(h_r^{-2}, h_\theta^{-2}, h_\phi^{-2}, h_t^{-2}\right)\mathbf{Q}^t$$

Wave radius increases at $R(t) = R_0 + v_w t$
h_r increases away from $R(t)$, h_t = constant
h_ϕ, h_θ similar to Cube-Cylinder Polar 2 case

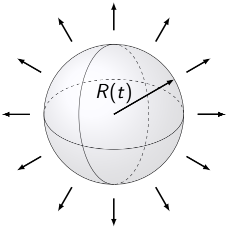

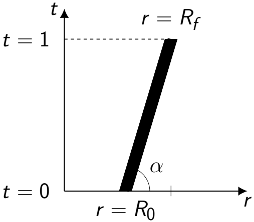

Let's look at some $4d$ metric-conforming cases in a tesseract.

Tesseract Linear

$$\mathbf{m}(\mathbf{x}) = \mathrm{diag}\left(h_x^{-2}, h_y^{-2}, h_z^{-2}, h_t^{-2}\right)$$

$h_x = h_y = h_z = h =$ constant
h_t increases away from $t = 0.5$.

TL1 ($h = 0.25$) **TL2** ($h = 0.125$)

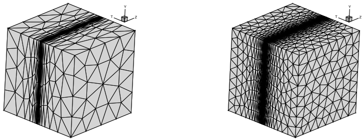

Refine hyperplanes at non-constant t.

Tesseract Wave

$$\mathbf{m}(\mathbf{x}) = \mathbf{Q}\,\mathrm{diag}\left(h_r^{-2}, h_\theta^{-2}, h_\phi^{-2}, h_t^{-2}\right)\,\mathbf{Q}^t$$

Wave radius increases at $R(t) = R_0 + v_w t$
h_r increases away from $R(t)$, $h_t =$ constant
h_ϕ, h_θ similar to Cube-Cylinder Polar 2 case

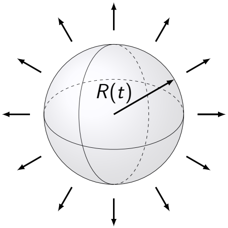

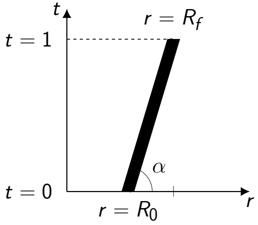

Refine spheres at constant t and cones at non-constant t.

We will look at *boundaries* of the tesseract meshes.

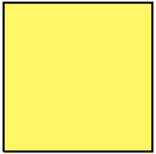

We will look at *boundaries* of the tesseract meshes.

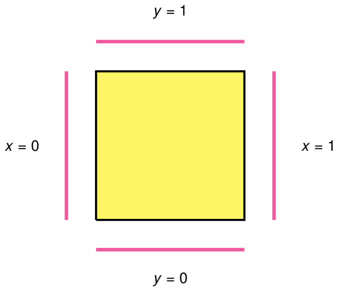

We will look at *boundaries* of the tesseract meshes.

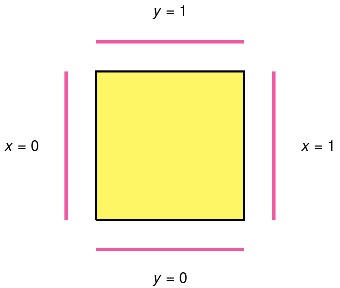

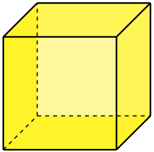

We will look at *boundaries* of the tesseract meshes.

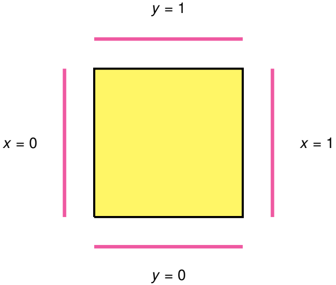

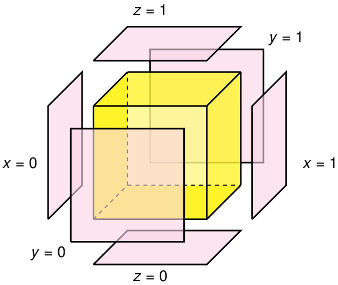

We will look at *boundaries* of the tesseract meshes.

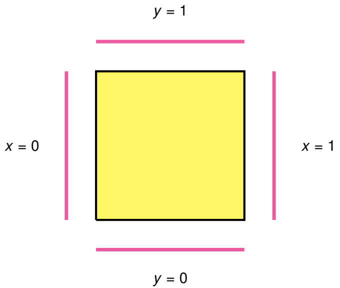

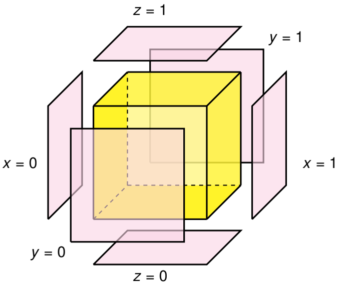

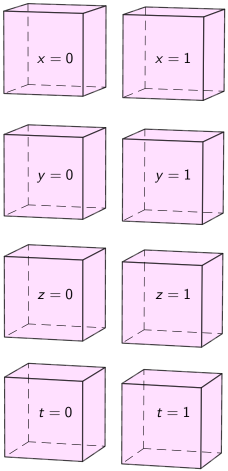

Expected hyperplanes are refined for the Tesseract Linear cases.

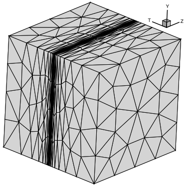

$x = 0$

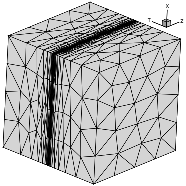

$y = 0$

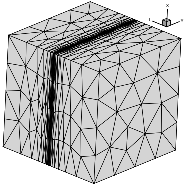

$z = 0$

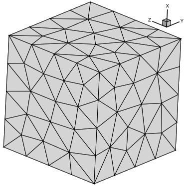

$t = 0$

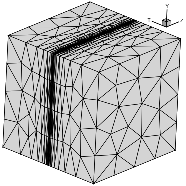

$x = 1$

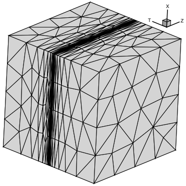

$y = 1$

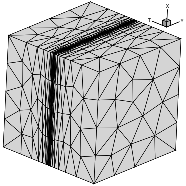

$z = 1$

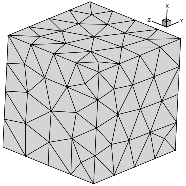

$t = 1$

Expected spheres and cones are refined for the Tesseract Wave case.

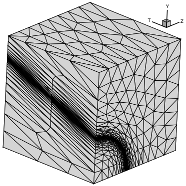

$x = 0$

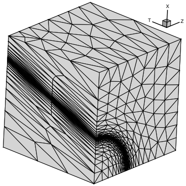

$y = 0$

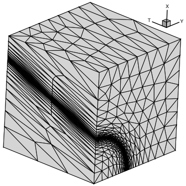

$z = 0$

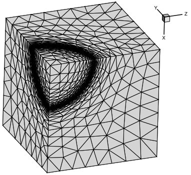

$t = 0$

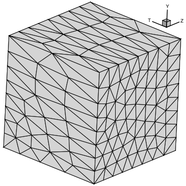

$x = 1$

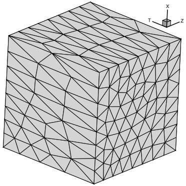

$y = 1$

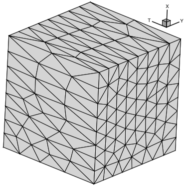

$z = 1$

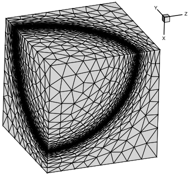

$t = 1$

Good metric-conformity is observed for the $4d$ benchmark cases.

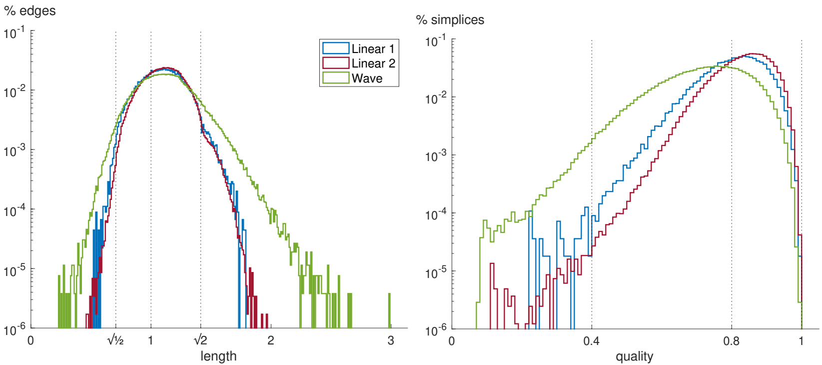

	$\%\ell_{\text{unit}}$	$\%q_{\text{unit}}$	# simplices	expected
Linear 1	96.46 %	56.35 %	55.66k	51k
Linear 2	97.27 %	70.00 %	814.50k	818k
Wave	88.96 %	26.89 %	347.19k	n/a

Demonstration within adaptive framework

MIT AEROASTRO

Metric fields obtained from MOESS [Yano, 2012].

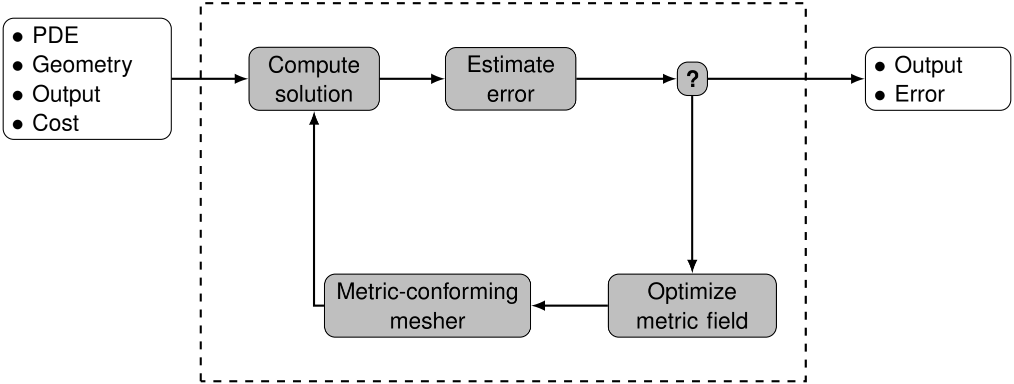

Metric fields obtained from MOESS [Yano, 2012].

MIT AEROASTRO

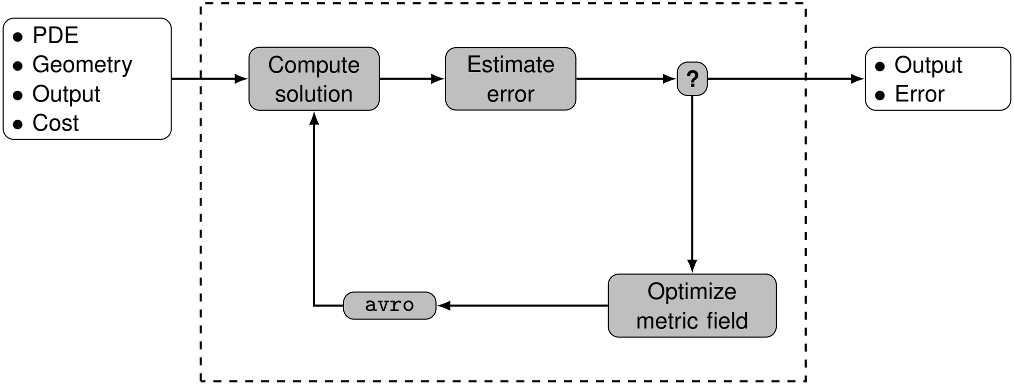

Metric fields obtained from MOESS [Yano, 2012].

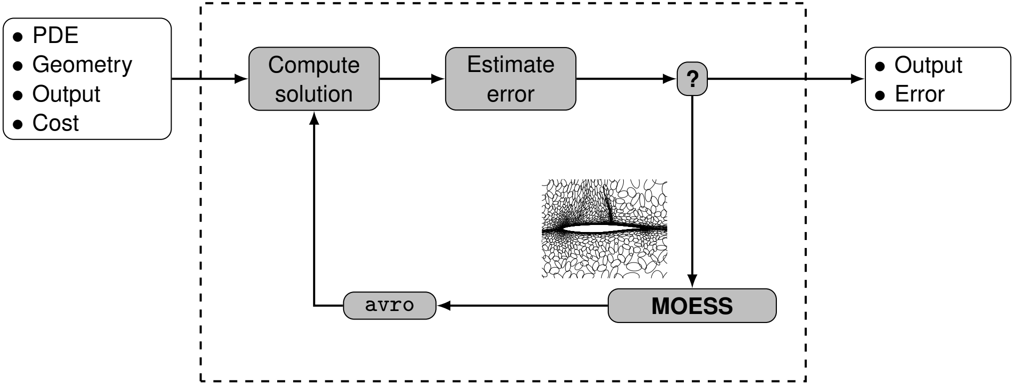

Metric fields obtained from MOESS [Yano, 2012].

Mesh Optimization via Error Sampling and Synthesis

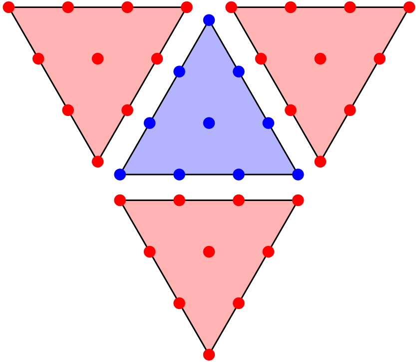

Original

Metric fields obtained from MOESS [Yano, 2012].

Mesh Optimization via Error Sampling and Synthesis

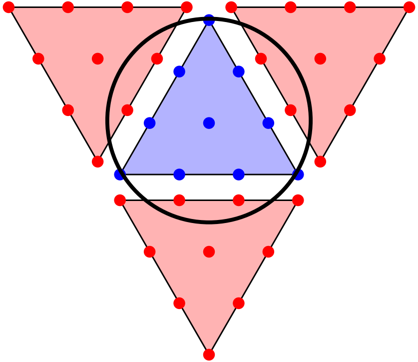

Original $\mathbf{m}_0$ η_0

Metric fields obtained from MOESS [Yano, 2012].

Mesh Optimization via Error Sampling and Synthesis

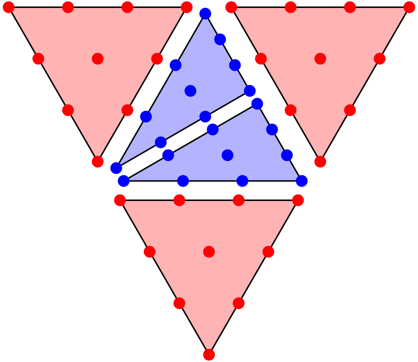

Original	$\mathbf{m}_0$	η_0
Edge split 1		

Metric fields obtained from MOESS [Yano, 2012].

Mesh Optimization via Error Sampling and Synthesis

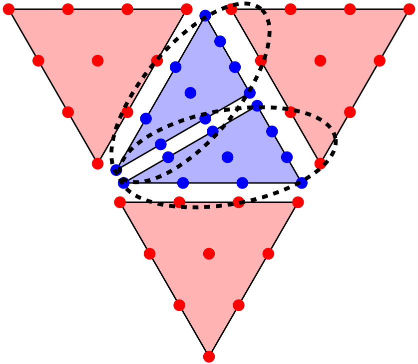

Original $\mathbf{m}_0$ η_0

Edge split 1

Metric fields obtained from MOESS [Yano, 2012].

Mesh Optimization via Error Sampling and Synthesis

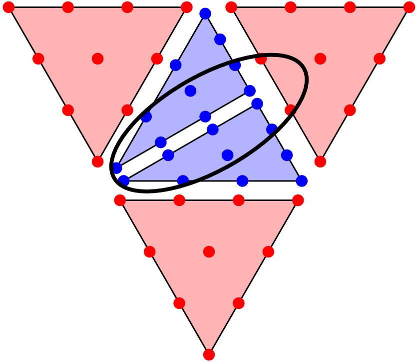

Original	$\mathbf{m}_0$	η_0
Edge split 1	$\mathbf{m}_1$	η_1

Metric fields obtained from MOESS [Yano, 2012].

Mesh Optimization via Error Sampling and Synthesis

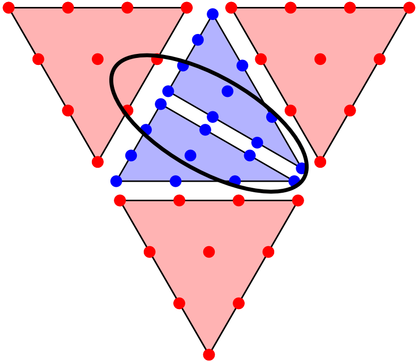

Original	$\mathbf{m}_0$	η_0
Edge split 1	$\mathbf{m}_1$	η_1
Edge split 2	$\mathbf{m}_2$	η_2

Metric fields obtained from MOESS [Yano, 2012].

Mesh Optimization via Error Sampling and Synthesis

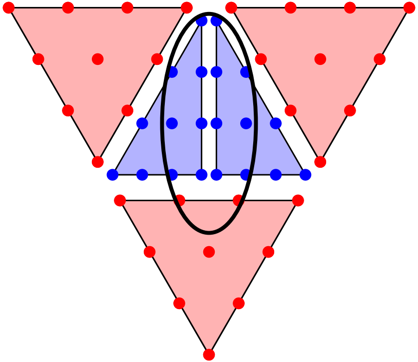

Original	$\mathbf{m}_0$	η_0
Edge split 1	$\mathbf{m}_1$	η_1
Edge split 2	$\mathbf{m}_2$	η_2
Edge split 3	$\mathbf{m}_3$	η_3

Metric fields obtained from MOESS [Yano, 2012].

Mesh Optimization via Error Sampling and Synthesis

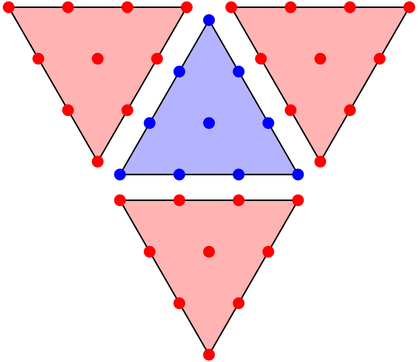

Original	$\mathbf{m}_0$	η_0
Edge split 1	$\mathbf{m}_1$	η_1
Edge split 2	$\mathbf{m}_2$	η_2
Edge split 3	$\mathbf{m}_3$	η_3

Error model: $\eta(\mathbf{s}) = \eta_0 \exp(\mathrm{tr}(\mathbf{r}\,\mathbf{s}))$

Adapt to the exact L^2 error.

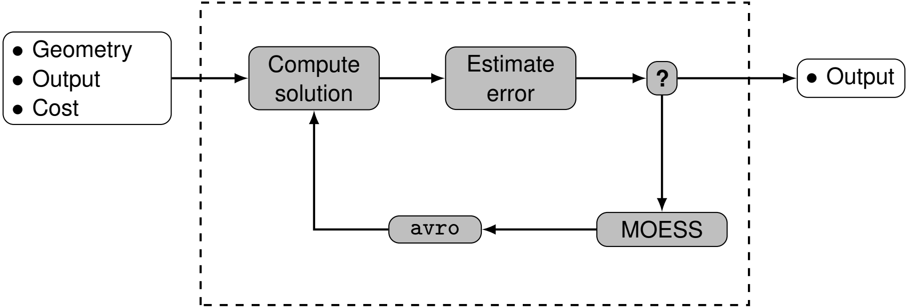

Adapt to the exact L^2 error of a boundary layer function.

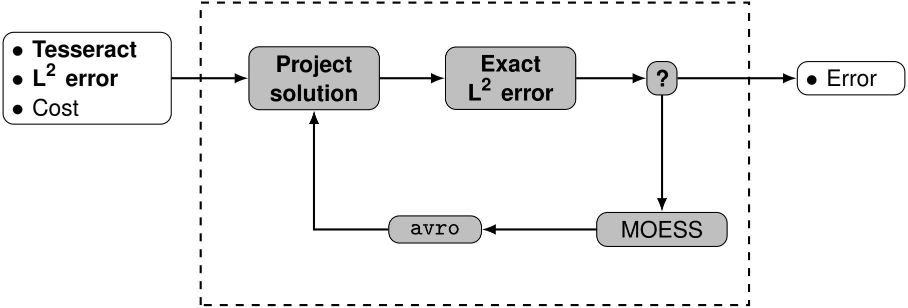

$$u(x,y,z,t) = \exp(-x/\epsilon) + \frac{(2y)^{p+1}}{(p+1)!} + \frac{(4z)^{p+1}}{(p+1)!} + \frac{(6t)^{p+1}}{(p+1)!} \quad \epsilon = 0.01$$

using $p = 1$ and $p = 2$ discontinuous Galerkin solution spaces

Optimal mesh size & aspect ratios [Yano, 2012]

$$h_x = h_{x,0} \exp(k_{h_x} x)$$

$$a_i = a_{i,0} \exp(k_a x), \;\; i = y, z, t$$

L^2 error control for boundary layer: DOF overshoot $\approx$ 35%.

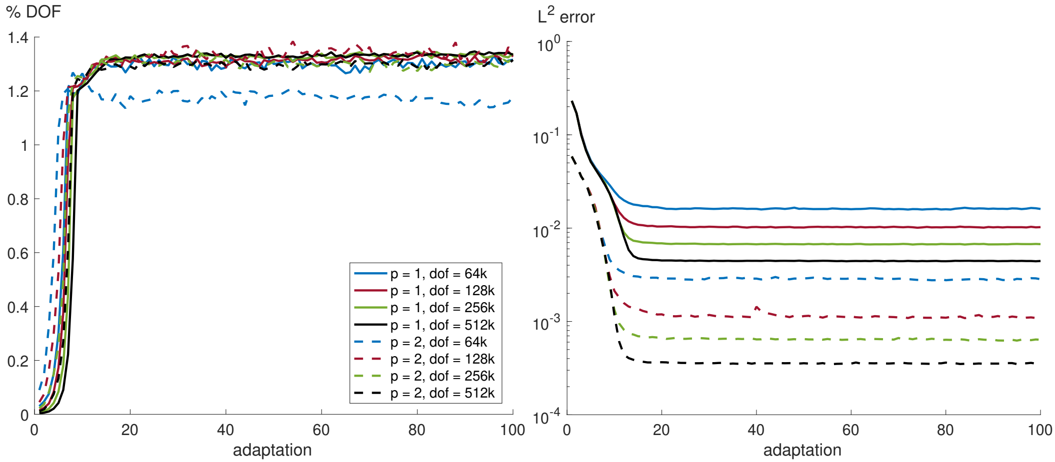

$p = 1$ 512k DOF optimized meshes show expected refinement.

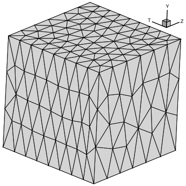

$x = 0$

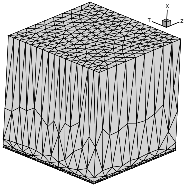

$y = 0$

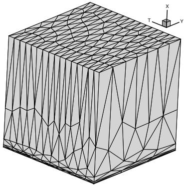

$z = 0$

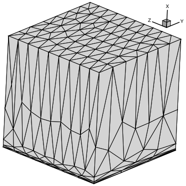

$t = 0$

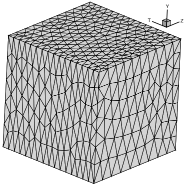

$x = 1$

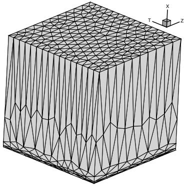

$y = 1$

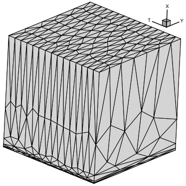

$z = 1$

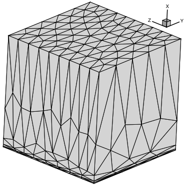

$t = 1$

p = 2 **512k DOF optimized meshes show expected refinement.**

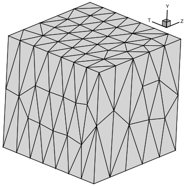

$x = 0$

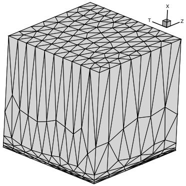

$y = 0$

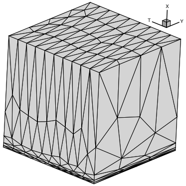

$z = 0$

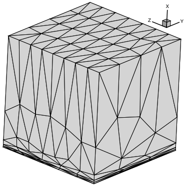

$t = 0$

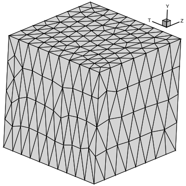

$x = 1$

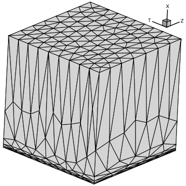

$y = 1$

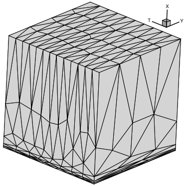

$z = 1$

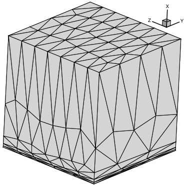

$t = 1$

Analytic mesh distributions achieved.

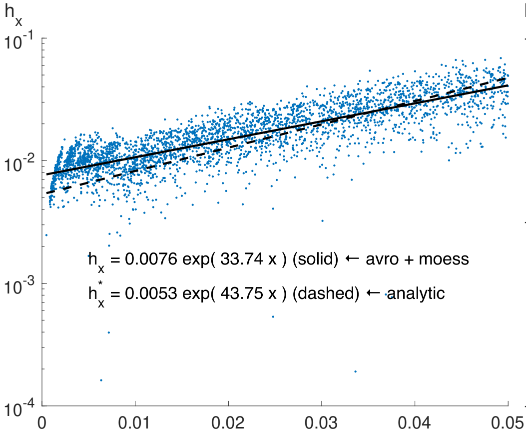

p = 1

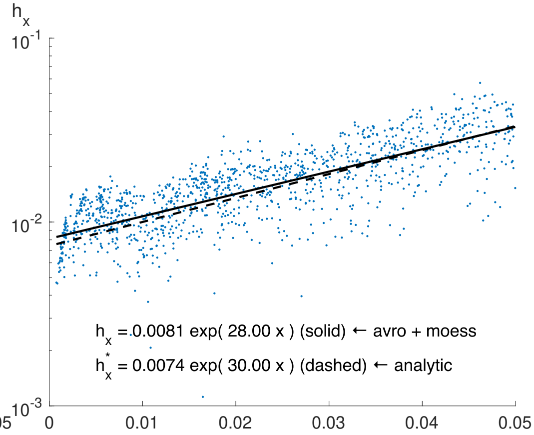

p = 2

Analytic mesh distributions achieved.

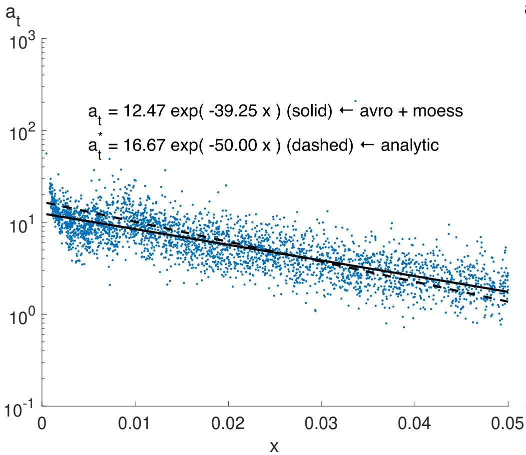

$p = 1$

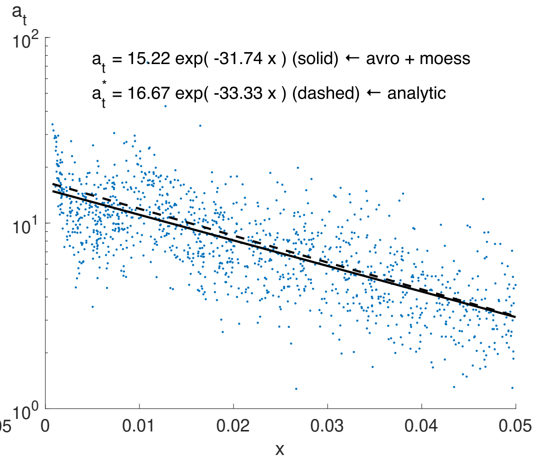

$p = 2$

Adapt to the exact L^2 error of a spherical wave function.

$$u(\mathbf{x}, t) = \exp(-t)\exp\left(-200(R(t) - ||\mathbf{x}||)^2\right) \quad \text{with } R(t) = 0.4 + 0.7t$$

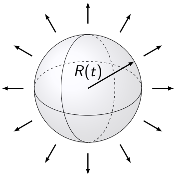

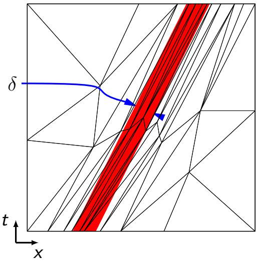

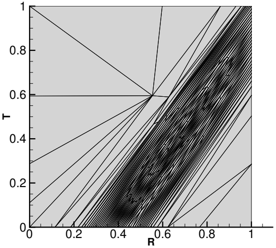

DOF overshoot complemented by slight rise in error.

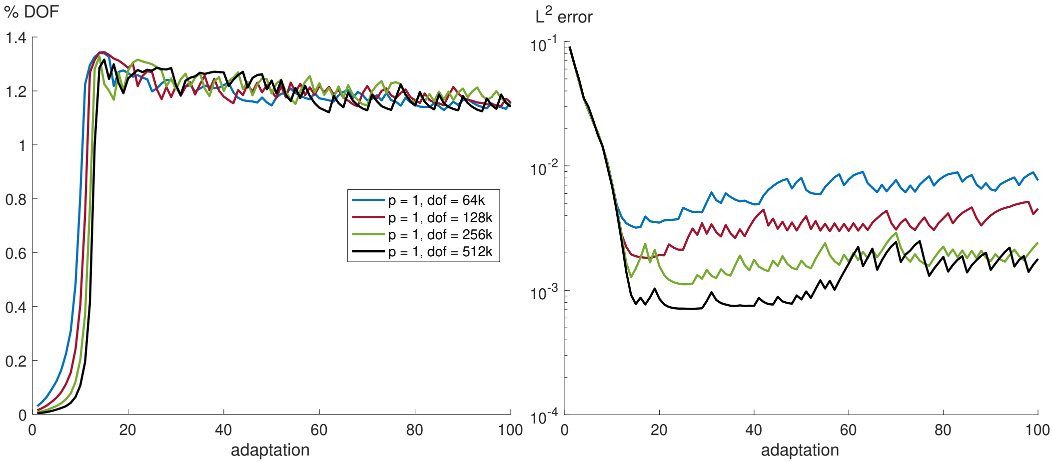

DOF overshoot complemented by slight rise in error.

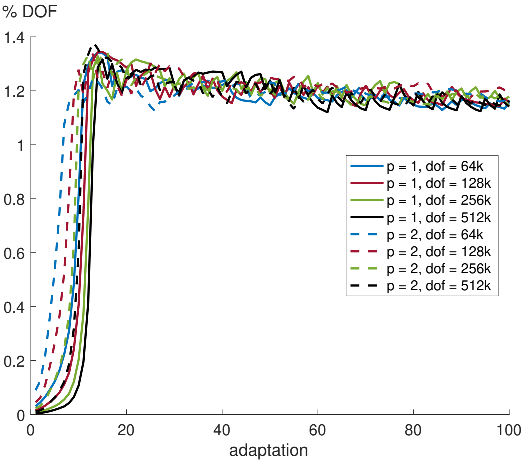

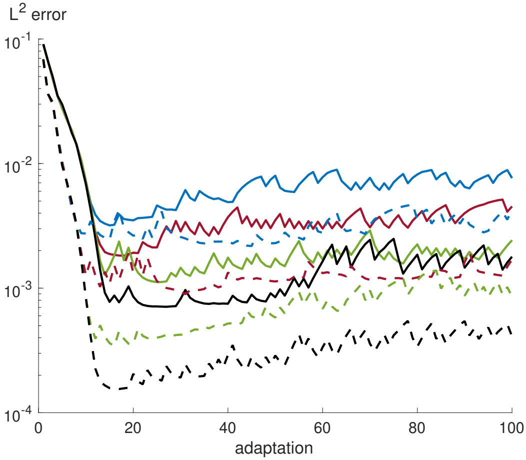

p = 1 **512k DOF optimized meshes show expected refinement.**

MIT AEROASTRO

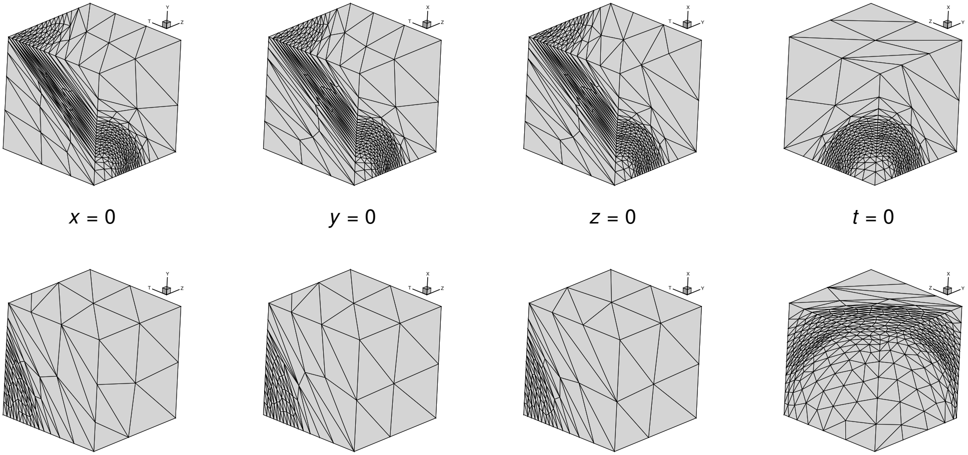

$x = 0$	$y = 0$	$z = 0$	$t = 0$
$x = 1$	$y = 1$	$z = 1$	$t = 1$

p = 2 **512k DOF optimized meshes show expected refinement.**

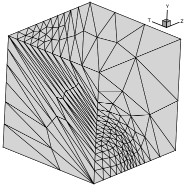

$x = 0$

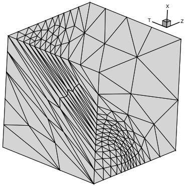

$y = 0$

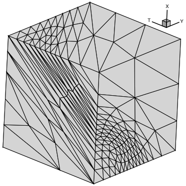

$z = 0$

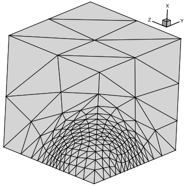

$t = 0$

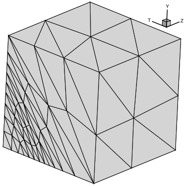

$x = 1$

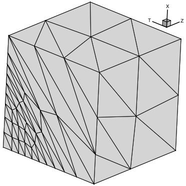

$y = 1$

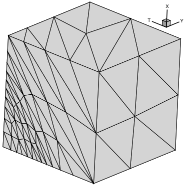

$z = 1$

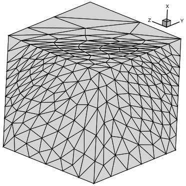

$t = 1$

Metric conformity is good.

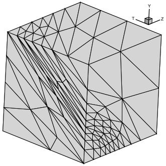

p = 1, 64k DOF

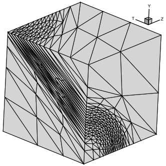

p = 1, 512k DOF

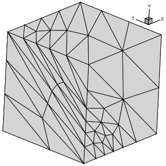

p = 2, 64k DOF

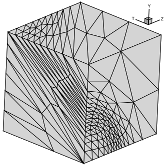

p = 2, 512k DOF

	$\%\ell_{\text{unit}}$	$\%q_{\text{unit}}$	# simplices	% overshoot
p = 1, 64k	97.72 %	53.31 %	14.83k	15.84 %
p = 1, 512k	97.57 %	51.76 %	116.86k	14.12 %
p = 2, 64k	98.71 %	50.15 %	4.87k	14.12 %
p = 2, 512k	97.40 %	49.63 %	39.76k	16.47 %

Large aspect ratios are obtained.

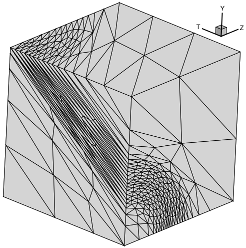

p = 1, 512k DOF

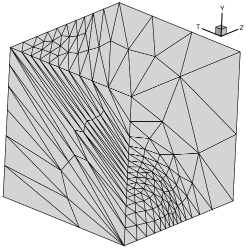

p = 2, 512k DOF

Order / DOF	64k	128k	256k	512k
p = 1	2.07e+02	5.07e+02	8.32e+02	2.12e+03
p = 2	6.53e+01	1.26e+02	2.60e+02	5.88e+02

Unsteady advection-diffusion with a boundary layer.

MIT AEROASTRO

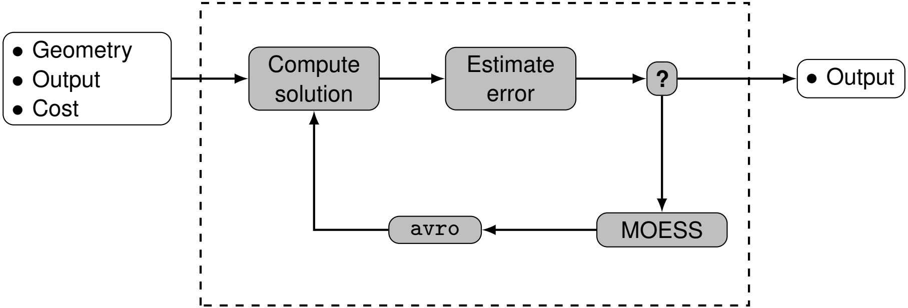

Unsteady advection-diffusion with a boundary layer.

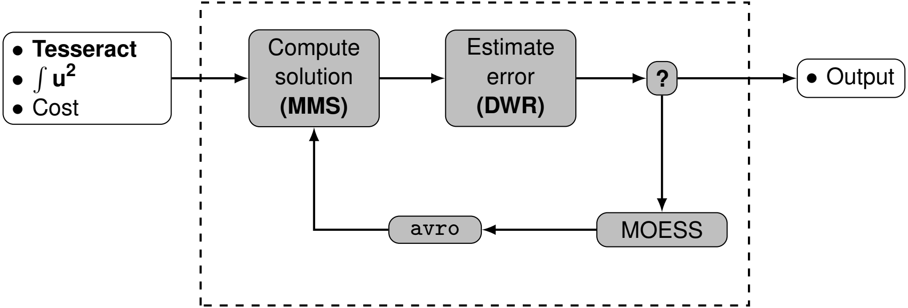

$$\frac{\partial u}{\partial t} + \nabla \cdot (\mathbf{c}\, u - \nabla u) = s(\mathbf{x}, t) \quad \mathbf{c} = (0.5, 0.5, 0.5)^t$$

$$u(x, y, z, t) = \exp(-x/\epsilon) + \frac{(2y)^{p+1}}{(p+1)!} + \frac{(4z)^{p+1}}{(p+1)!} + \frac{(6t)^{p+1}}{(p+1)!} \quad \epsilon = 0.01$$

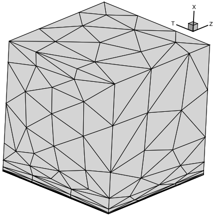

DOF overshoot as high as 43%.

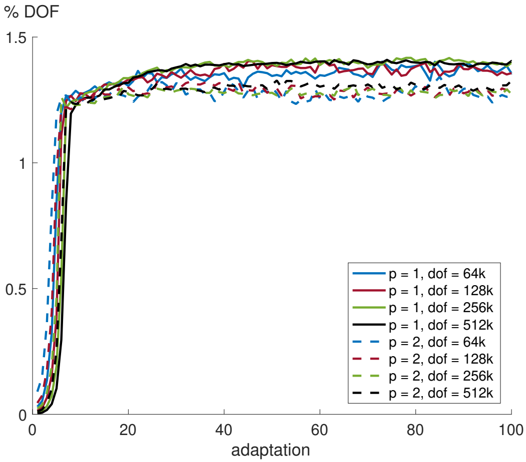

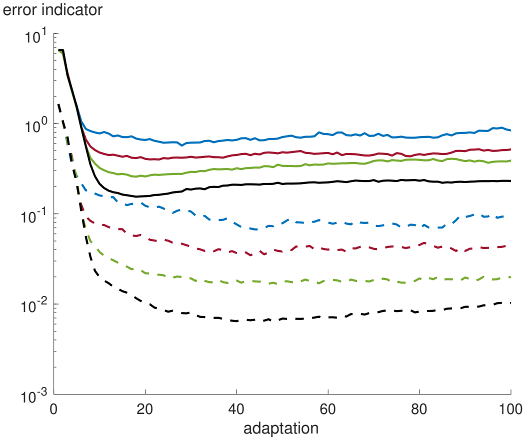

$p = 2$ **512k DOF optimized meshes show expected refinement.**

MIT AEROASTRO

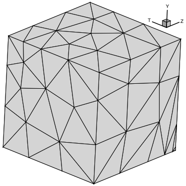

$x = 0$

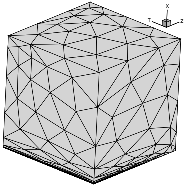

$y = 0$

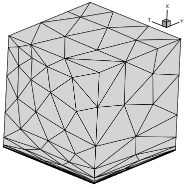

$z = 0$

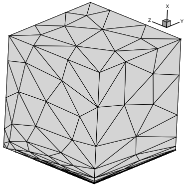

$t = 0$

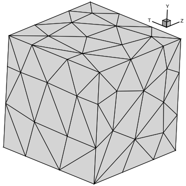

$x = 1$

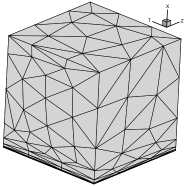

$y = 1$

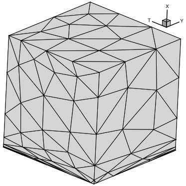

$z = 1$

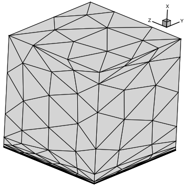

$t = 1$

Unsteady advection-diffusion with an expanding spherical wave.

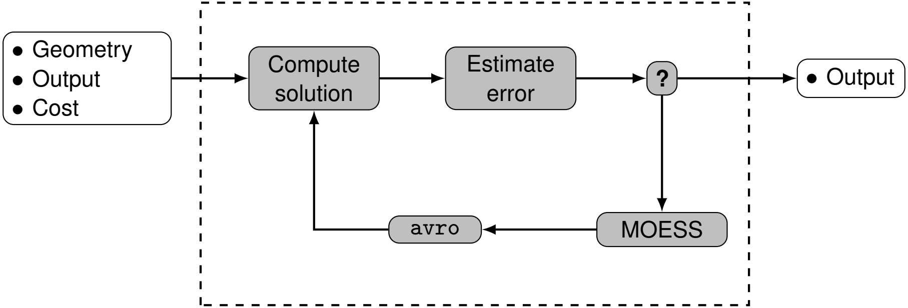

Unsteady advection-diffusion with an expanding spherical wave.

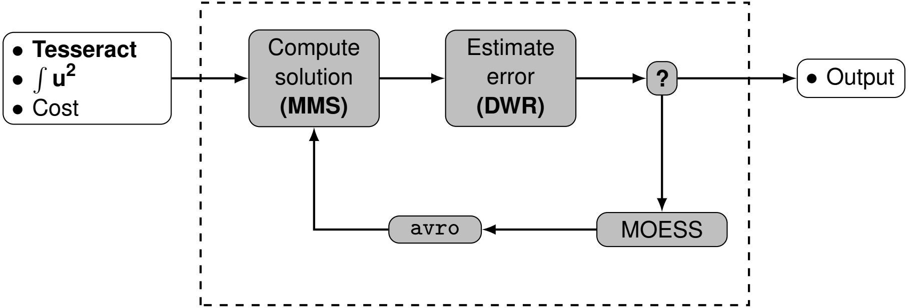

$$\frac{\partial u}{\partial t} + \nabla \cdot (\mathbf{c}\, u - \nu \nabla u) = s(\mathbf{x}, t) \quad \mathbf{c} = 0.5\mathbf{e}_r, \;\; \nu = 0.01$$

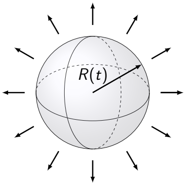

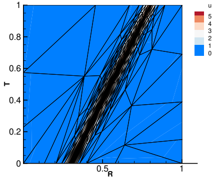

$$u(\mathbf{x}, t) = 5\exp(-0.1t)\exp\left(-1000(R(t) - ||\mathbf{x}||)^2\right) \qquad R(t) = 0.3 + 0.5t$$

DOF overshoot as high as 38%.

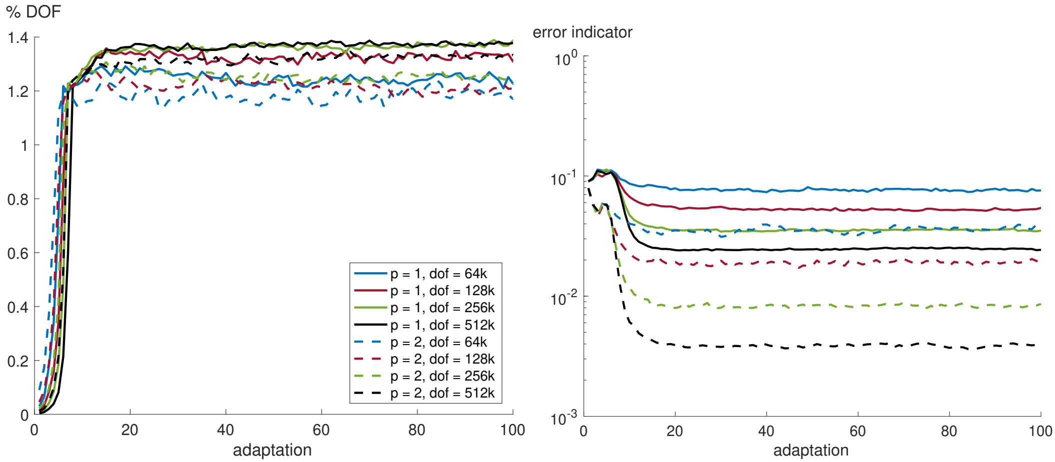

$p = 1$ 512k DOF optimized meshes show expected refinement.

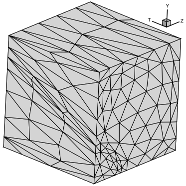

$x = 0$

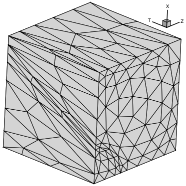

$y = 0$

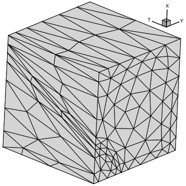

$z = 0$

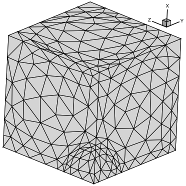

$t = 0$

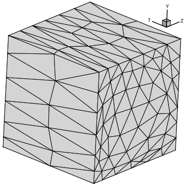

$x = 1$

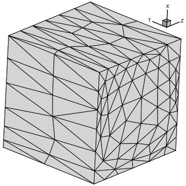

$y = 1$

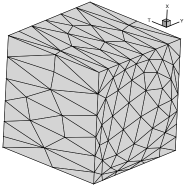

$z = 1$

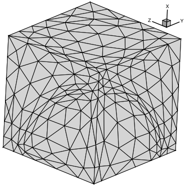

$t = 1$

Need more DOF to fully refine solution.

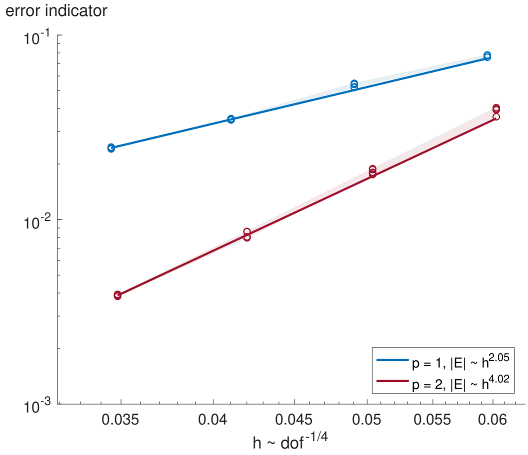

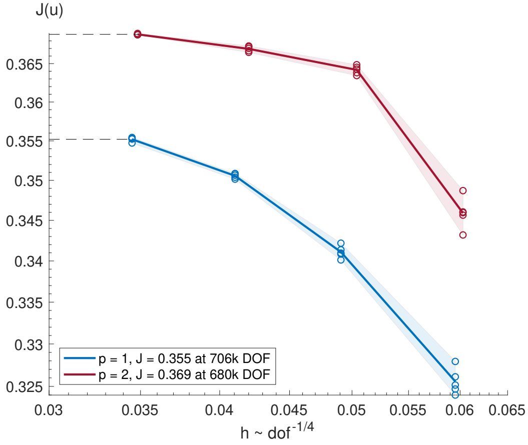

Spherical wave at $t = 1$ is captured.

Conclusions

MIT AEROASTRO

Summary

Main objective:

Develop an anisotropic four-dimensional meshing capability for adaptive numerical simulations.

Contributions:

(1) Develop an algorithm and software for 4d **metric-conforming mesh adaptation**.

(2) **Validate the adaptive algorithm** on 4d problems.

(3) Demonstrate first **PDE-driven anisotropic** unstructured adaptation for **unsteady** 3d **problems**.

Summary

Main objective:

Develop an anisotropic four-dimensional meshing capability for adaptive numerical simulations.

Contributions:

(1) Develop an algorithm and software for $4d$ **metric-conforming mesh adaptation**.

(2) **Validate the adaptive algorithm** on $4d$ problems.

(3) Demonstrate first **PDE-driven anisotropic** unstructured adaptation for **unsteady** $3d$ **problems**.

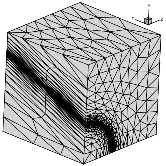

metric-conforming

Summary

Main objective:

Develop an anisotropic four-dimensional meshing capability for adaptive numerical simulations.

Contributions:

(1) Develop an algorithm and software for 4*d* **metric-conforming mesh adaptation.**

(2) **Validate the adaptive algorithm** on 4*d* problems.

(3) Demonstrate first **PDE-driven anisotropic** unstructured adaptation for **unsteady** 3*d* **problems.**

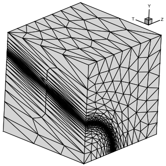

metric-conforming

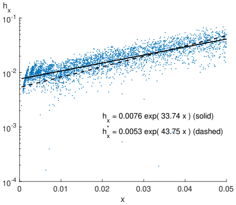

validation

Summary

Main objective:

Develop an anisotropic four-dimensional meshing capability for adaptive numerical simulations.

Contributions:

(1) Develop an algorithm and software for 4*d* **metric-conforming mesh adaptation.**

(2) **Validate the adaptive algorithm** on 4*d* problems.

(3) Demonstrate first **PDE-driven anisotropic** unstructured adaptation for **unsteady** 3*d* **problems.**

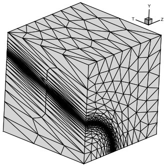

metric-conforming

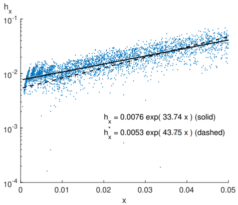

validation

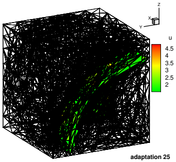

PDE-driven

AEROASTRO MIT

Main objective:

Develop an anisotropic four-dimensional meshing capability for adaptive numerical simulations.

Contributions:

(1) Develop an algorithm and software for 4*d* **metric-conforming mesh adaptation.**

(2) **Validate the adaptive algorithm** on 4*d* problems.

(3) Demonstrate first **PDE-driven anisotropic** unstructured adaptation for **unsteady** 3*d* **problems.**

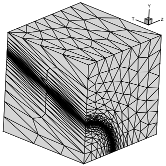

metric-conforming

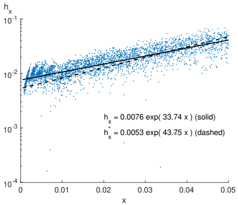

validation

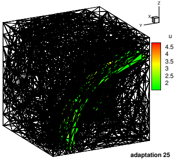

PDE-driven

`avro`

Future work

- **Parallelization** of the mesh adaptation algorithm,
- Adaptation of **curvilinear** meshes,
- Applications of the framework to **other PDEs**,
- Investigating **continuous Galerkin** discretization,
- Mesh adaptation for **higher-dimensional parameter spaces**.

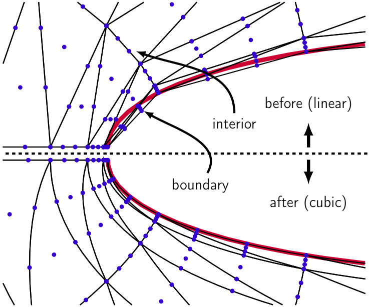

Acknowledgements

This work was funded by the CAPS project: **AFRL Contract FA8050-14-C-2472**:
CAPS: Computational Aircraft Prototype Syntheses with Dean Bryson as technical monitor.

Acknowledgements

This work was funded by the CAPS project: **AFRL Contract FA8050-14-C-2472**:
CAPS: Computational Aircraft Prototype Syntheses with Dean Bryson as technical monitor.

Acknowledgements

This work was funded by the CAPS project: **AFRL Contract FA8050-14-C-2472**:
CAPS: Computational Aircraft Prototype Syntheses with Dean Bryson as technical monitor.

MIT Hyperloop
David Darmofal
Carmen
Steve Allmaras Eloi
Ryan
Janice Ursa Xevi Roca
Cory
Alex Tek Grandpapa
Ellie
Nisha
Zanna Victor Mike Hugh
Patrick Sarthak Abel Nani
Guillem Dave Robertson
Jun
Dot Max Dad Ben Savithru
Jean
Rohith Juliana Qiqi
Shun Mike Park Jaime Peraire
Maman
Sreeja Bob Julia Ferran Irina Marshall
Caroline Eric Dow Catherine
Steve Ojeda Grandmaman
Arthur Todd Billings

Ryan & Alex

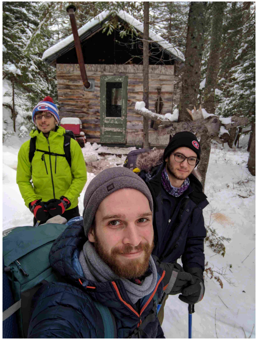

Acknowledgements

This work was funded by the CAPS project: **AFRL Contract FA8050-14-C-2472**:
CAPS: Computational Aircraft Prototype Syntheses with Dean Bryson as technical monitor.

Ryan & Alex

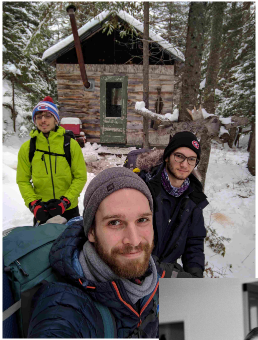

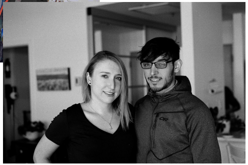

Catherine

Acknowledgements

This work was funded by the CAPS project: **AFRL Contract FA8050-14-C-2472**:
CAPS: Computational Aircraft Prototype Syntheses with Dean Bryson as technical monitor.

MIT Hyperloop
David Darmofal Carmen
Steve Allmaras Eloi
Ryan
Janice Ursa Xevi Roca
Cory
Alex Tek Grandpapa Ellie
Nisha
Zanna Victor Mike Hugh
Patrick Sarthak Abel Nani
Guillem Dave Robertson
Jun
Dot Max Dad Ben Savithru
Jean
Rohith Juliana Qiqi
Shun Mike Park Jaime Peraire
Maman Marshall
Sreeja Bob Julia Ferran Irina
Caroline Eric Dow Catherine
Steve Ojeda Grandmaman
Arthur Todd Billings

Questions?

References (1)

[Bangerth, 1999] Bangerth, W. (1999).
Finite element approximation of the acoustic wave equation: error control and mesh adaptation.
East-West Journal of Numerical Mathematics, 7(4):263–282.

[Coupez, 2000] Coupez, T. (2000).
Génération de maillage et adaptation de maillage par optimisation locale.
Revue européenne des éléments finis, 9:403–423.

[Frey and George, 2008] Frey, P. and George, P. (2008).
Mesh generation: Application to finite elements: Second edition.
Mesh Generation: Application to Finite Elements: Second Edition.

[Gruau, 2005] Gruau, C. (2005).
Metric generation for anisotropic mesh adaptation, with numerical applications to material forming simulation.
PhD thesis, École Nationale Supérieure des Mines de Paris.

[Hartmann, 2001] Hartmann, R. (2001).
Adaptive FE methods for conservation equations.
In Freistühler, H. and Warnecke, G., editors, Hyperbolic Problems: Theory, Numerics, Applications: Eighth International Conference in Magdeburg, February, March 2000, volume 141 of International series of numerical mathematics, pages 495–503. Birkhäuser, Basel.

[Ibanez et al., 2017] Ibanez, D., Barral, N., Krakos, J., Loseille, A., Michal, T., and Park, M. (2017).
First benchmark of the unstructured grid adaptation working group.
Procedia Engineering, 203:154 – 166.
26th International Meshing Roundtable, IMR26, 18-21 September 2017, Barcelona, Spain.

[Jayasinghe, 2018] Jayasinghe, S. (2018).
An adaptive space-time discontinuous Galerkin method for reservoir flows.
PhD thesis, Massachusetts Institute of Technology, Department of Aeronautics and Astronautics.

[Johnson, 2005] Johnson, F. T. (2005).
Computer and Fluids, 34:1115–1151.

[Kallus, 2011] Kallus, Y. (2011).
Solving Geometric Puzzles With Divide And Concur.
PhD thesis.

References (2)

[Loseille, 2011] Loseille, A. (2011).
Continuous mesh framework part I: Well-posed continuous interpolation error.
49(1):38–60.

[Loseille, 2017] Loseille, A. (2017).
Unique cavity-based operator and hierarchical domain partitioning for fast parallel generation of anisotropic meshes.
Computer-Aided Design, 85:53 – 67.
24th International Meshing Roundtable Special Issue: Advances in Mesh Generation.

[Song, 2014] Song, J. (2014).
Three-dimensional flow and lift characteristics of a hovering ruby-throated hummingbird.
Journal of The Royal Society Interface, 11.

[Tremblay, 2007] Tremblay, P. (2007).
2-D, 3-D and 4-D Anisotropic Mesh Adaptation for the Time-Continuous Space-Time Finite Element Method with Applications to the Incompressible Navier-Stokes Equations.
PhD thesis.

[Yano, 2012] Yano, M. (2012).
An Optimization Framework for Adaptive Higher-Order Discretizations of Partial Differential Equations on Anisotropic Simplex Meshes.
PhD thesis, Massachusetts Institute of Technology, Department of Aeronautics and Astronautics.

Why the giraffe?

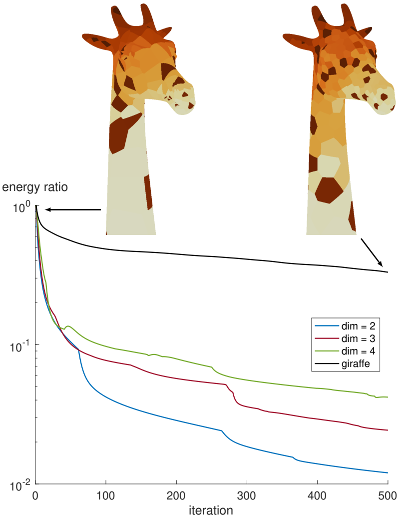

Why the giraffe?

MIT AEROASTRO

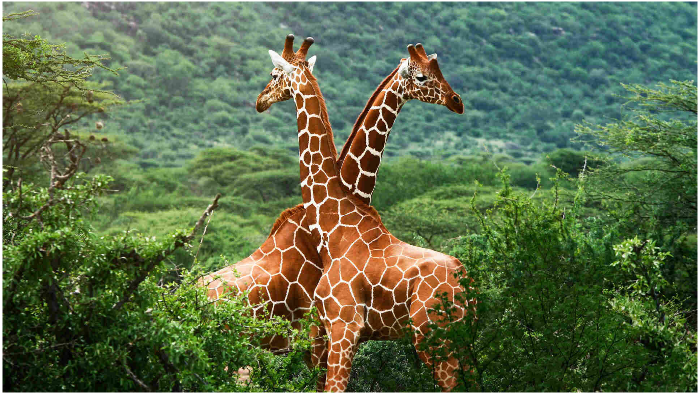

Why the $\sqrt{2}$?

[Frey and George, 2008]: *The coefficient $\sqrt{2}$ is related to the fact that an edge can be split if the lengths of the two sub-edges minimize the error distance to the unit length as compared with the initial length.*

In other words:

- We want to minimize ℓ_{split}:

$$\ell_{\text{split}} = \arg\min_{\alpha} \; \alpha \quad \text{such that } g(\alpha) = 2\left(\frac{\alpha}{2} - 1\right)^2 - (\alpha - 1)^2 \leq 0$$

  Applying the KKT conditions leads to $g(\alpha) = 0 \rightarrow \ell_{\text{split}} = \sqrt{2}$.

- We want to maximize ℓ_{collapse} but if we make it too big, then we will cycle between splitting and collapsing because splitting can create edges with length $\ell_{\text{split}}/2$. We can avoid this by setting $\ell_{\text{collapse}} = \sqrt{2}/2$.

Study of mesh adaptation components

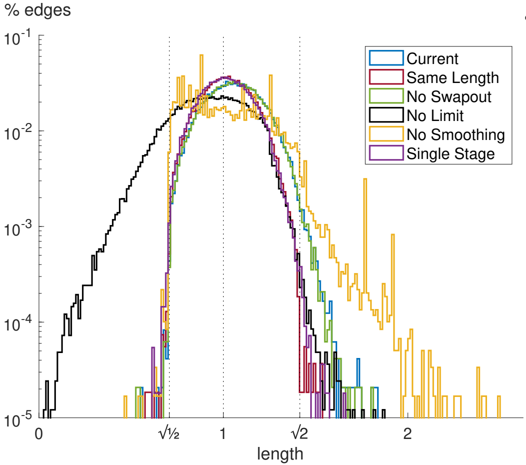

Edge lengths

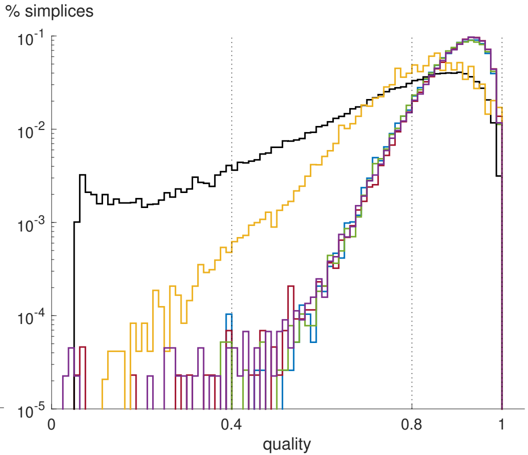

Simplex quality

Study of mesh adaptation components

Property	Current	Variant 1 Same Length	Variant 2 No Swapout	Variant 3 No Limit	Variant 4 No Smoothing	Variant 5 Single Stage
ℓ_{min}	0.67	0.57	0.64	0.06	0.58	0.55
ℓ_{max}	1.77	1.66	1.69	1.62	2.50	1.72
ℓ_{avg}	1.06	1.03	1.06	0.95	1.03	1.02
$\%\ell_{\text{unit}}$	99.10 %	99.92 %	99.06 %	89.60 %	96.48 %	99.74 %
q_{min}	0.47	0.09	0.46	0.10	0.09	0.17
q_{avg}	0.90	0.90	0.90	0.80	0.83	0.90
$\%q_{\text{unit}}$	92.15 %	93.46 %	92.08 %	62.45 %	67.44 %	92.25 %
# simplices	38.30k	42.67k	38.20k	58.62k	47.65k	43.60k

Visualizing slices of a $4d$ mesh

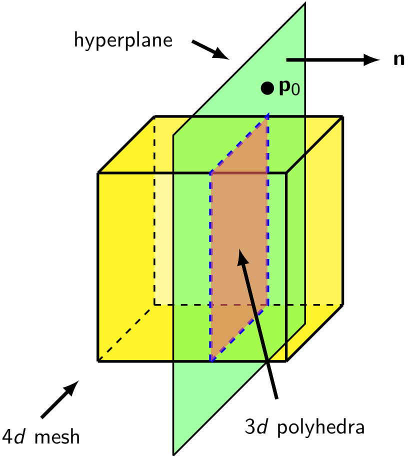

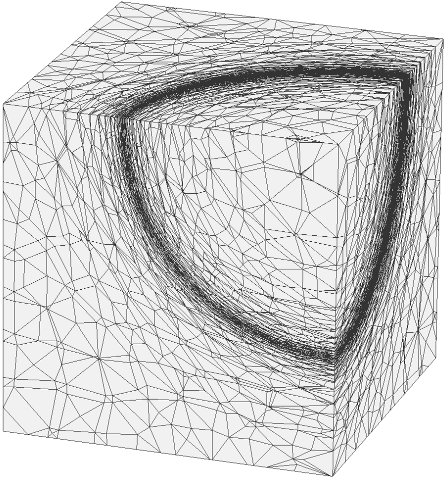

Why so much overshoot?

Valency statistics

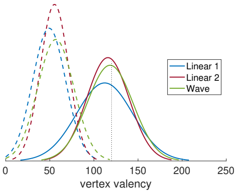

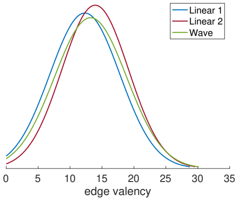

Packing fraction

Packing fraction (ϕ) defined as volume fraction of space covered by particles.

Best known packing fractions of unit-length equilateral simplices **[Kallus, 2011]**:

$$\phi_3 = 100/117 \approx 85.47\%$$

$$\phi_4 = 128/219 \approx 58.45\%$$

Maintaining a valid mesh

Theory

Definition of a mesh topology:
Let $\mathcal{V}$ be a set of vertices in some domain Ω and $\mathcal{T}$ be a set of n-polytopes with vertices in $\mathcal{V}$. Let $\mathcal{F}$ be the set of faces $(n-1)$-facets of $\mathcal{T}$. $\mathcal{T}$ is called a *mesh topology* if

(1) $\text{card}(f \cap \mathcal{T}) \leq 2,\ \forall f \in \mathcal{F}$,

(2) $(\mathcal{V}, \partial\mathcal{T})$ is a mesh of $\partial\Omega$.

Practice

(1) Close the mesh by connecting boundary to a ghost vertex.

(2) Check inserted elements do not already exist in $\mathcal{T}$.

(3) Use neighbour relations to ensure every facet touches two elements.

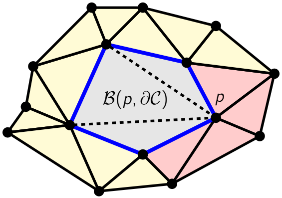

Convergence of the L^2 error for simple problem.

Adapting to L^2 error in solution:

$$u(x, y, z, t) = \exp(-5t) \sin 2\pi x \sin 2\pi y \sin 2\pi z$$

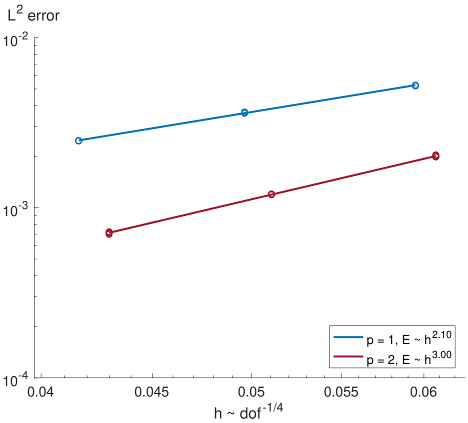

Geometry metadata is important to determine validity of operators.

- **Collapse edge** $e = (p, q)$: $g_q \preceq g_p$,
- **Insert vertex** p along edge e: $g_p \leftarrow g_e$,
- **Swap edge** e with re-insertion vertex p: $g_p \preceq g_e$,
- **Smooth vertex** p: driven by lengths of edges (p, q) surrounding p such that $g_q \preceq g_p$.

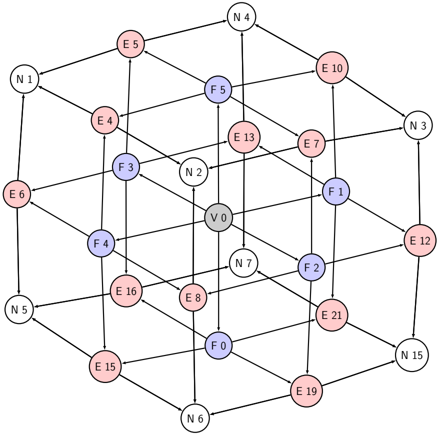

Difference in $4d$ benchmarks with or without DOF control.

Property	Linear 1 (no control)	Linear 2 (no control)	Wave (no control)	Linear 1 (control)	Linear 2 (control)	Wave (control)
ℓ_{min}	0.50	0.40	0.20	0.53	0.47	0.23
ℓ_{max}	1.91	1.86	2.71	1.78	1.96	2.99
ℓ_{avg}	1.08	1.08	1.08	1.10	1.11	1.12
$\%\ell_{\text{unit}}$	97.29 %	98.01 %	92.48 %	96.46 %	97.27 %	88.96 %
q_{min}	0.16	0.02	0.02	0.23	0.11	0.08
q_{avg}	0.80	0.83	0.72	0.80	0.83	0.72
$\%q_{\text{unit}}$	56.67 %	67.13 %	28.75 %	56.35 %	70.00 %	26.89 %
# simplices	59.56k	915.30k	394.07k	55.66k	814.50k	347.19k
expected	51.00k	818.00k	n/a	51.00k	818.00k	n/a

Mesh size and aspect ratio distributions for L^2 boundary layer case

Coefficient	Analytic	64k	128k	256k	512k
$h_{x,0}$	$h^*_{x,0}$	0.0155	0.0121	0.0095	0.0076
$h^*_{x,0}$	-	0.0090	0.0075	0.0063	0.0053
k_{h_x}	43.75	25.14	28.39	31.29	33.74
$a_{y,0}$	50.00	25.52	29.46	32.15	33.76
k_{a_y}	-50.00	-26.57	-31.14	-35.22	-38.05
$a_{z,0}$	25.00	14.32	16.02	17.09	18.18
k_{a_z}	-50.00	-26.84	-31.79	-35.92	-38.92
$a_{t,0}$	16.67	9.59	10.75	11.76	12.47
k_{a_t}	-50.00	-26.11	-31.44	-35.58	-39.25

$p = 1$

Coefficient	Analytic	64k	128k	256k	512k
$h_{x,0}$	$h^*_{x,0}$	0.0146	0.0119	0.0100	0.0081
$h^*_{x,0}$	-	0.0125	0.0105	0.0088	0.0074
k_{h_x}	30.00	25.46	24.56	27.36	28.00
$a_{y,0}$	50.00	38.06	42.92	40.45	44.13
k_{a_y}	-33.33	-24.69	-28.12	-29.80	-31.04
$a_{z,0}$	25.00	22.41	21.51	22.11	22.06
k_{a_z}	-33.33	-25.96	-27.69	-30.55	-30.68
$a_{t,0}$	16.67	15.39	14.55	14.64	15.22
k_{a_t}	-33.33	-26.60	-28.50	-30.14	-31.74

$p = 2$

Advection-diffusion boundary layer convergence rates

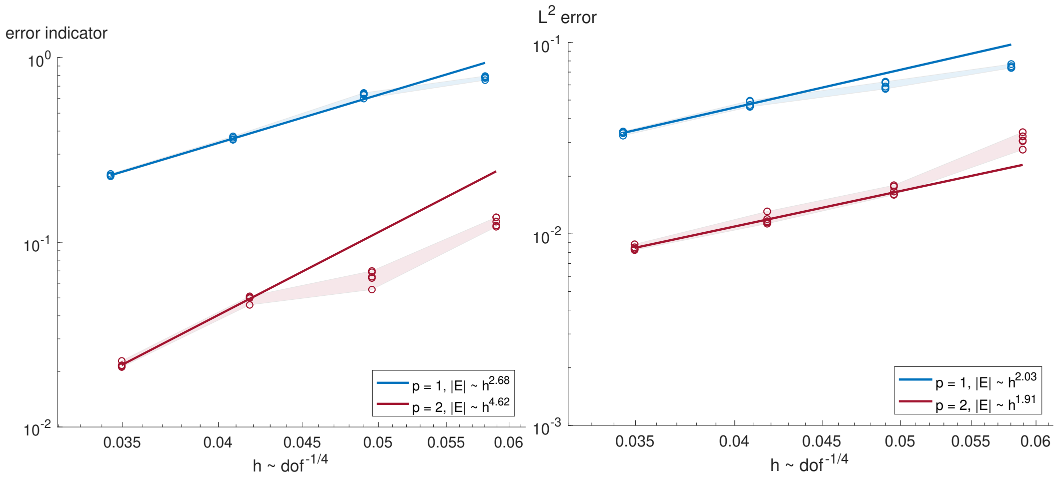

Boundary layer (advection-diffusion) $p = 2$ meshes.

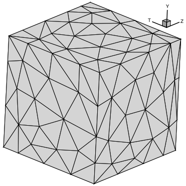

$x = 0$

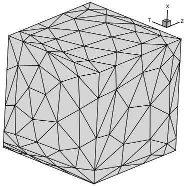

$y = 0$

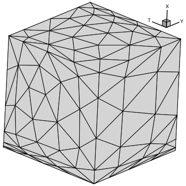

$z = 0$

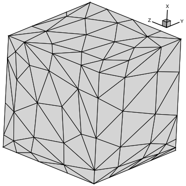

$t = 0$

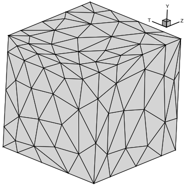

$x = 1$

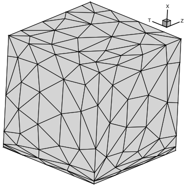

$y = 1$

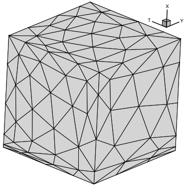

$z = 1$

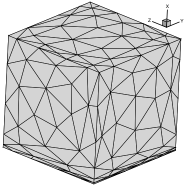

$t = 1$

Spherical wave (advection-diffusion) $p = 2$ meshes.

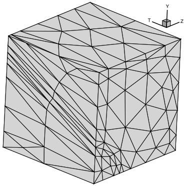

$x = 0$

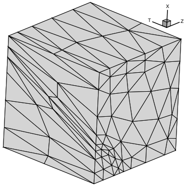

$y = 0$

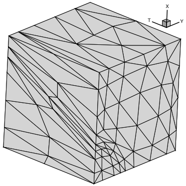

$z = 0$

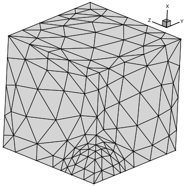

$t = 0$

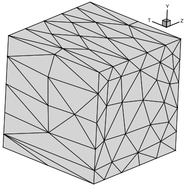

$x = 1$

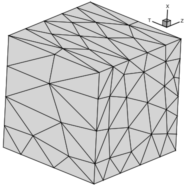

$y = 1$

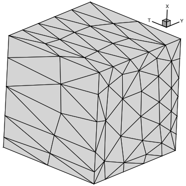

$z = 1$

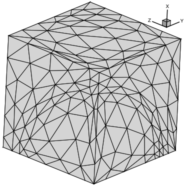

$t = 1$